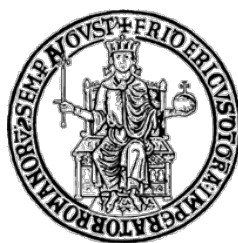


UNIVERSITÀ DEGLI STUDI DI NAPOLI

“FEDERICO II”

DEPARTMENT OF CHEMICAL, MATERIALS AND INDUSTRIAL
PRODUCTION ENGINEERING

XXIX cycle



PhD in “INDUSTRIAL PRODUCTS AND PROCESSES ENGINEERING”

“Multifunctional polymeric nanocapsules via
layer by layer on oil based liquid templates”

Supervisor

Prof. Paolo Antonio Netti

Advisor

Dott. Ing. Raffaele Vecchione

Coordinator

Prof. Giuseppe Mensitieri

PhD student

Giulia Iaccarino

2014/2017

Table of Contents

| | |
|--|-----------|
| Chapter 1..... | 5 |
| Theoretical Background..... | 5 |
| 1.1 Nanotechnology, Nanomedicine and Drug Delivery..... | 6 |
| 1.2 Aim of the work and thesis outline..... | 11 |
| 1.3 References..... | 13 |
| Chapter 2..... | 15 |
| Ultrastable Polyelectrolyte Multilayer Lipid nanocapsules..... | 15 |
| Abstract..... | 16 |
| 2.1 Introduction..... | 17 |
| 2.2 Results and Discussion..... | 22 |
| Nanoemulsions are reliable liquid templates..... | 22 |
| Multilayer deposition on oil-core nanocapsules..... | 25 |
| Nanocapsules number of layers affects their biological applications..... | 29 |
| 2.3 Conclusions..... | 31 |
| 2.4 Materials and Methods..... | 33 |
| Materials..... | 33 |
| Nanoemulsion template preparation..... | 33 |
| Polyelectrolytes multilayer deposition..... | 34 |
| Particle size and Z-potential characterization..... | 36 |
| Cryo-TEM characterization of the system..... | 36 |
| STED analysis of nanocapsules..... | 37 |
| Cytotoxicity assay..... | 38 |
| Cell uptake analysis..... | 39 |
| 2.5 Supplementary Section..... | 40 |
| Saturation method..... | 40 |
| Zetasizer analysis of multilayer nanocapsules..... | 41 |
| Stability over time of multilayer nanocapsules..... | 44 |
| 2.6 References..... | 45 |
| Chapter 3..... | 49 |
| Stimuli-responsive oil-core nanocapsules..... | 49 |
| Abstract..... | 50 |
| 3.1 Introduction..... | 51 |
| 3.2 Results and Discussion..... | 55 |
| Solid phase peptide synthesis..... | 55 |

| | |
|---|-----------|
| Heparin – rhodamine peptide conjugation | 57 |
| Glycolated chitosan thiolation with N-acetyl-L-cysteine | 59 |
| Stability enhancement of MMP-2 trilayer nanocapsules | 62 |
| Cytotoxicity and Confocal Microscopy Imaging of MMP-2 Sensitive nanocapsules | 64 |
| 3.3 Conclusions | 69 |
| 3.4 Future Perspectives..... | 70 |
| 3.5 Materials and Methods..... | 71 |
| Materials..... | 71 |
| Peptide synthesis..... | 72 |
| Labeling reaction | 72 |
| Heparin - peptide coupling reaction..... | 73 |
| Oil-in-Water nanoemulsion | 74 |
| Modification of glycol chitosan with N-Acetylcysteine..... | 74 |
| LbL deposition of functionalized polymers on O/W nanoemulsion | 75 |
| LbL deposition of functionalized polymers on polystyrene carboxylated nanoparticles | 76 |
| Photoreaction of the multilayer | 76 |
| Particle size and Z-potential characterization | 76 |
| Stability tests on crosslinked and not crosslinked trilayers | 77 |
| Confocal analysis of trilayer nanocapsules | 77 |
| Cell culture..... | 77 |
| Nanocapsules in vitro enzymatic treatment..... | 78 |
| Cell viability..... | 79 |
| Confocal microscopy imaging of MMP-2 sensitive nanocapsules in cells | 79 |
| 3.6 References | 81 |
| Chapter 4..... | 83 |
| Graphene oxide oil-core nanocapsules | 83 |
| 4.1 Introduction | 85 |
| 4.2 Results and Discussion | 92 |
| Graphene oxide modification and its deposition on O/W nanoemulsions | 92 |
| 4.3 Conclusions | 100 |
| 4.4 Future Perspectives..... | 101 |
| 4.5 Materials and Methods..... | 102 |
| Materials..... | 102 |
| Oil-in-Water nanoemulsion | 102 |
| Chemical and structural modification of graphene oxide | 103 |
| LbL deposition of modified graphene oxide on O/W nanoemulsions | 103 |
| Particle size and Z-potential measurements | 104 |
| XPS analysis..... | 104 |
| Cryo-TEM analysis..... | 104 |
| Cell culture and sample preparation | 105 |
| GO nanocapsules imaging in living cells | 106 |
| 4.6 References | 107 |

Chapter 5..... 111
Conclusions 111

Chapter 1

Theoretical Background

1.1 Nanotechnology, Nanomedicine and Drug Delivery

Over the last decade the application of nanotechnology to medicine is completely reshaping our idea of therapy and diagnostic. It is common knowledge that standard therapeutic approaches may suffer from poor efficacy and several side effects. Cancer, for example, as a major cause of death needs new therapeutic approaches, which target the disease and avoid drug resistance. Nanomedicine, and in particular drug delivery systems (DDS), promise to address unmet medical needs in cancer and other diseases. This exciting interdisciplinary *arena* lies at the intersection of different research areas such as engineering, biotechnology, and material science [1]. Someone glimpses into nanomedicine the avenues for a sort of next industrial revolution, which will improve both the health and wealth of nations. Among the most impressive future trends I would mention *personalized medicine*, which has the ambition of tailoring health care to each person's unique genetic makeup [2]. Also, another breakthrough that may change our perception of healthcare is the creation of *point-of-care* (POC), capable of bringing the laboratory diagnostic test outside of traditional care settings [3]. POC devices may be simple enough to be used at the primary care level and in remote settings with no laboratory infrastructure. These solutions potentially enable patients to self-test in the privacy of their homes.

It must be pointed out, though, that the lack of scientific information on health risk and the challenges on translational research might postpone this “nanorevolution” [3, 4]. Whatever your view, nanotechnology is invading virtually every segment of industry. Mind how it is entering everybody's home through mobile phones, computer and other high technology devices. It is thanks to advances in nanolithography, for example, that transistors get smaller and smaller and computer processors consequently faster [2]. Also, you may

likely find a nanotechnology-based product among your cosmetics. Skin creams and other lotions often contain nano sized parcels of ingredients (as in the case of liposomes) to improve the solubility of ingredients and add shimmer [5]. Moreover, a process frequently used for the formulation of cosmetics is nanoemulsion (NE), by which one liquid disperses in nanoscale droplets throughout the other. The derived fine texture allow for the transport of beneficial compounds deep into the skin and in high concentrations [6]. The list might go on and on ranging from energy to coating and paints and many other sectors.

However, while the future is happening, how many average citizens could give a definition of nanoscience, nanobiotechnology, nanomedicine, nanocosmetics, nanomaterial, nanocarrier, nanoelectronics and so on? True is that there is still much confusion in defining the *nano* world as it usually happens with emerging technologies. The word *nano* comes from Greek and stands for *dwarf*. Thereby, nanoscience deals with the study of molecules and objects which can be measured in nanometers (billionths of meter or 10^{-9} m). The birth and development of nanotechnology is still unclear, although naïve applications of nanoscience can be traced to medieval glaziers. By a nanofabrication process they produced the gold nanodots, which were responsible for the color of the famous glass windows of ancient churches. As far as the modern origin of nanotechnology, it is easier to converge toward one name, the Nobel Prize Richard Feynman. During the most famous lecture he was giving at the annual meeting of the American Physics Society at Caltech in 1959, he pointed at the different problems that can affect the miniaturization process since “all things do not simply scale down in proportion”. At the nanoscale different laws apply, so we have to expect different things to happen. Gravity becomes much less relevant and things stick together by molecular van der Waals attractions. Also, Feynman was the first to introduce the concept of *bottom-up* approach to the fabrication of miniaturized device such as integrated circuits. To witness another

leap in nanotechnology we have to wait quite a few years. It is the 1981 when in the IBM labs they invent a new microscope capable to move a sharp tip so close to a conductive surface that the wave functions of the atoms of the surface and of the tips overlap. By applying a voltage electrons can “tunnel” the vacuum gap between the surface and the tip [7]. The *Scanning Tunneling Microscope* (STM) paved the way for another technique of scanning probe microscopy, namely the *Atomic Force Microscopy* (AFM), which is today very common for imaging, force measurement, and manipulation of matter at the nanoscale [8]. These powerful instruments for the investigation of the nanoscale are capable to resolve matter far beyond optical diffraction limit and both deserved a Nobel Prize.

Therefore, we can define nanotechnology as the ability of manipulating and exploring matter on a nanometer scale length down to atomic dimensions. The nanoscale brings to materials and molecular assemblies different physical and chemical properties, thus introducing new features for therapeutic and diagnostic applications. The lifelong concern of mankind for improving human health has eventually brought the new field of nanomedicine to blossom from the application of nanotechnology cues to medicine. This interdisciplinary research area has given a strong boost to the development of new diagnostic and therapeutic strategies trying to address the major issues of medicine [9]. Conventional anticancer therapies, for example, are known to be plagued by severe side effects and poor efficacy. The main reason behind these drawbacks is due to the lack of selectivity of therapeutic agents for the diseased tissues. Thereby, in spite of accumulating mostly at the target site, the drug interacts indiscriminately with the rest of the body killing also the healthy tissues and significantly decreasing the effective therapeutic dose. The need to maximize the biodistribution and pharmacokinetics of therapeutic agents has led to the development of nanosized DDS acting as reservoirs capable to protect the human body from the adverse effect of drugs and *vice-versa* [10]. During blood circulation, indeed, drugs encounter several barriers hindering their route to the

target site, such as the uptake from the reticuloendothelial system (RES). This network of phagocytic cells disseminated throughout the body plays a role in clearing the blood from unwanted foreign material. Thus, ideal DDS should be stable enough to allow for the accumulation of the encapsulated drug in the target tissue, while masking its payload from body clearance [11].

Another constraint for an effective delivery strategy deals with the dimensions that DDS may possibly achieve. In fact size matters! From deep insight into tumor biology, leaky blood vessels and dysfunctional lymphatic drainage emerged as characteristic features consequence of rapid and defective angiogenesis. Unlike the free drug, which may diffuse non-specifically, nanocarriers with a size of about 100 nm can extravasate into the tumor tissues escaping through the fenestration of the defective vessels. Then, thanks to the dysfunctional lymphatic drainage it is retained close to the tumor cells where it can release the drug (for a schematic representation see **Figure 1.1**) resulting in the so called permeability and retention effect (EPR) [12]. One can take advantage of this pathophysiological cue of tumors for the rational design of DDS which can passively accumulate at the diseased tissue. This is only one representative example of how medicine and nanotechnology met half way to foster new strategies for improving therapies. Designing nanocarriers with the right size is just the first requirement to potentially translate the DDS into the clinics. Then, several other properties of the nanocarriers can be modified to positively affect their therapeutic efficacy. These include biocompatibility and biodegradability, drug release mechanism and biodistribution.

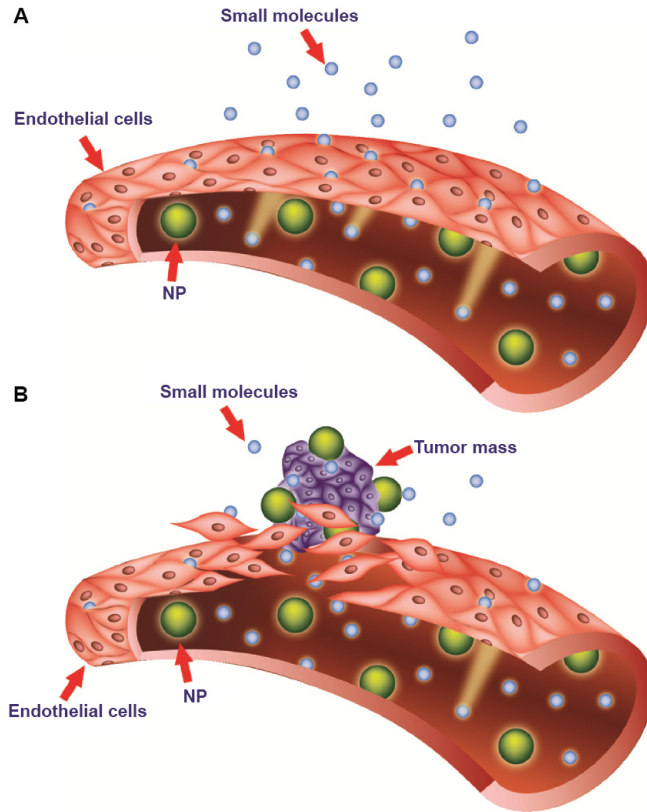


Figure 1.1 Targeting of nanomedicines by the enhanced permeability and retention (EPR) effect. Notes: Differences between normal (A) and tumor (B) vessels are depicted. Tumor vessels contain large fenestrations between the endothelial cells: this structural characteristic allows the nanoparticles (NPs) to reach the matrix and the tumor cells by the EPR effect. Conversely, normal tissue contains tightly joined endothelial cells: this prevents the diffusion of NPs outside the blood vessels. (Figure redrawn after ref [13]).

1.2 Aim of the work and thesis outline

Conventional therapeutic approaches are plagued by some major limitations which nanomedicine promises to address combining the advances in medicine and biology with nanotechnology based drug delivery systems. Novel nanocarriers are being developed to sidestep fundamental problems of traditional drugs based on their ability to overcome poor water solubility issues, improve physical/chemical stability, enhance bioavailability and alter unacceptable toxicity profiles. In particular, the Holy Grail of any drug delivery system is to transport the required dose of a particular active agent to a specific disease or tissue site throughout the body and release it in a controlled fashion. This strategy should ultimately lead to minimizing toxic side effects and optimizing therapeutic benefit. Nevertheless, the application of engineered nanodrugs into the clinics still proves challenging due to some bottlenecks, especially at the translational level.

Trying to give our own piece of contribution to this area of research, here we devoted the efforts toward the formulation of multifunctional drug delivery systems based on highly controllable liquid nanocapsules (NCs). We particularly drew the focus on the development of a robust and scalable technique to produce oil-core multilayer nanocarriers capable to encapsulate lipophilic agents of interest for nanomedicine. This methodology was a reliable platform for the implementation of further functionalities of great importance for drug delivery such as *stimuli*-responsive drug release mechanisms.

In **Chapter 2** we present an extensive work on the optimization of both the NE process and the layer-by-layer (LbL) deposition of naturally derived polymers at the liquid-liquid interface. This consolidated approach allowed for the preparation of versatile and highly controlled NCs with reproducible dimensional features (size \approx 100 nm; PDI $<$ 0.1). Thanks to their oil-core these NCs can pre-load several hydrophobic drugs overcoming tedious post-

processing procedures. We proved our method to be flexible also employing different materials for NCs preparation.

Moving from the results reported in **Chapter 3**, we upgraded the presented NCs to enhance their physical stability and to allow for spatially controlled release of chemotherapeutic agents. To achieve a *stimuli*-responsive release we chose an endogenous trigger which is characteristic of the nature of tumors microenvironment itself. The NCs were, indeed, finely engineered to be sensitive to the activity of particular enzymes overexpressed by several tumors.

Finally, in **Chapter 4** we present an early study on the integration of graphene oxide (GO) into NCs for drug delivery and bioimaging applications. As a derived form of graphene, GO exhibits many appealing and non-conventional features that might be of huge impact for nanomedicine.

1.3 References

- [1] V. Wagner, A. Dullaart, A.-K. Bock, A. Zweck, The emerging nanomedicine landscape, *Nat Biotech* 24(10) (2006) 1211-1217.
- [2] U. Food, D. Administration, Paving the way for personalized medicine: FDA's role in a new era of medical product development, Silver Spring, MD: US Food and Drug Administration (2013).
- [3] A. Larsson, R. Greig-Pylypczuk, A. Huisman, The state of point-of-care testing: a european perspective, *Upsala Journal of Medical Sciences* 120(1) (2015) 1-10.
- [4] M. Kendall, I. Lynch, Long-term monitoring for nanomedicine implants and drugs, *Nature nanotechnology* 11(3) (2016) 206-10.
- [5] M. Anis, G. AlTaher, W. Sarhan, M. Elsemary, *Cosmetic Applications, Nanovate, Springer*2017, pp. 243-260.
- [6] M.N. Yukuyama, D.D.M. Ghisleni, T.J.A. Pinto, N.A. Bou-Chacra, Nanoemulsion: process selection and application in cosmetics – a review, *International Journal of Cosmetic Science* 38(1) (2016) 13-24.
- [7] G. Binnig, H. Rohrer, Scanning tunneling microscopy—from birth to adolescence, *reviews of modern physics* 59(3) (1987) 615.
- [8] G. Binnig, C.F. Quate, C. Gerber, Atomic force microscope, *Physical review letters* 56(9) (1986) 930.
- [9] B. Müller, M.H. Van de Voorde, M. Van de Voorde, Benefit from Nanoscience and Nanotechnology: Benefitting Patients, *Nanoscience and Nanotechnology for Human Health* (2017) 379-382.
- [10] R. Zeineldin, J. Syoufjy, *Cancer Nanotechnology: Opportunities for Prevention, Diagnosis, and Therapy*, in: R. Zeineldin (Ed.), *Cancer Nanotechnology: Methods and Protocols*, Springer New York, New York, NY, 2017, pp. 3-12.
- [11] S. Manoochehri, B. Darvishi, G. Kamalinia, M. Amini, M. Fallah, S.N. Ostad, F. Atyabi, R. Dinarvand, Surface modification of PLGA nanoparticles via human serum albumin conjugation for controlled delivery of docetaxel, *Daru : journal of Faculty of Pharmacy, Tehran University of Medical Sciences* 21(1) (2013) 58.
- [12] Y. Matsumura, H. Maeda, A new concept for macromolecular therapeutics in cancer chemotherapy: mechanism of tumoritropic accumulation of proteins and the antitumor agent smancs, *Cancer research* 46(12 Pt 1) (1986) 6387-92.
- [13] G. Bozzuto, A. Molinari, Liposomes as nanomedical devices, *International journal of nanomedicine* 10 (2015) 975-99.

Chapter 2

Ultrastable Polyelectrolyte Multilayer Lipid nanocapsules

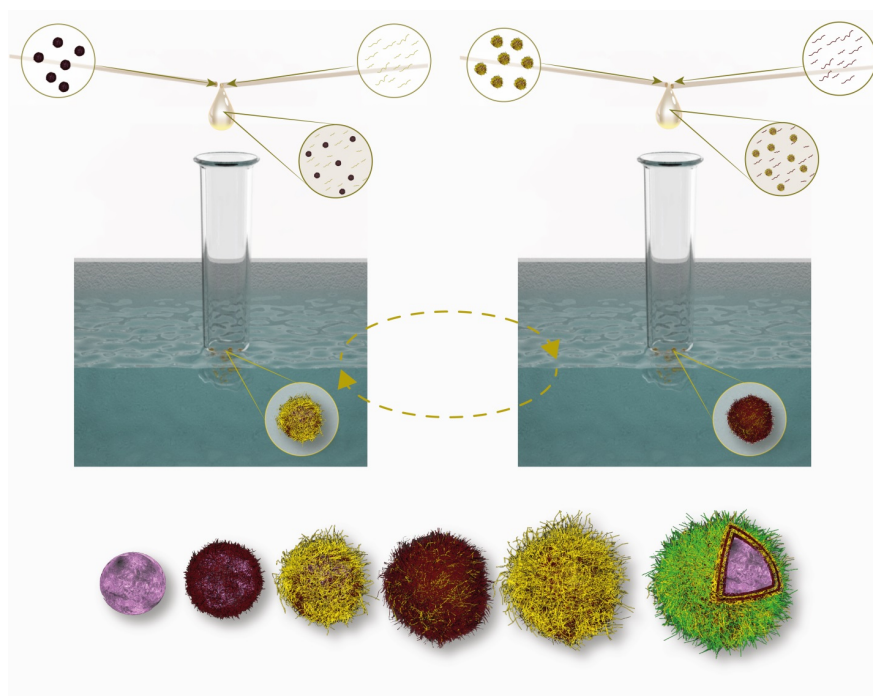


Figure 2.1 Scheme of the multilayer deposition on pre-loaded ultra-stable liquid template by means of sonication in a water bath of the two phases – polymer solution and suspension, which are injected dropwise.

Abstract

Liquid-liquid interfaces possess unique properties such as high interfacial tension and fluidity, which provide enhanced mobility for the achievement of an equilibrium assembly. Therefore, they are ideal templates for the preparation of polyelectrolyte multilayer nanocapsules. Drug delivery would particularly benefit from biodegradable polymer nanocapsules since they combine tunable shell properties with a liquid oily core capable to encapsulate high amounts of lipophilic payloads. However, governing the self-assembly of polyelectrolytes at the interface between to immiscible liquids can prove challenging due to the intrinsic instability and high reactivity of these systems. Here we report on the development of a robust platform for the preparation of ultrastable oil-core multilayer nanocapsules based on the optimization of both the nanoemulsion process and the Layer-by-Layer deposition technique. Our nanocapsules exhibit highly controlled dimensional features as highlighted by advanced morphological characterization. Moreover, they may be assembled with several naturally derived polymers and encapsulate a number of hydrophobic molecules thus showing multi-compartment and multifunctional features. These results together with their biocompatible nature may enrich their area of application in drug delivery, as well as in other bio-nanotechnology fields.

2.1 Introduction

Finely controlled biodegradable nanocapsules (NCs) are today highly demanded for several applications such as drug delivery, cosmetic, food and agriculture [1-5]. The main benefits coming from the encapsulation of actives are for protection of the entrapped substances from adverse environment, for controlled release, and for precision targeting. All these features make NCs particularly desirable as drug delivery systems capable of positively altering both the pharmacokinetics and the biodistribution of the drugs.

Moreover, today a bunch of new candidate molecules emerging from drug discovery show poor water solubility, which represents an additional constraint to the delivery of these actives throughout the body [6]. Again, nanotechnology-based formulations seem to be a smart answer to the improvement of drugs therapeutic performance thanks to the solubility enhancement they can provide through the core/shell architecture of nanocapsular systems. In fact, by masking hydrophobic drugs within a nanocavity with a hydrophilic external interface, one can dramatically improve the blood solubility of a wide range of therapeutics such as hydrophobic molecules, peptides, and oligonucleotides [7, 8]. This means in turn, enhancing drug bioavailability, lowering the required dose and thus reducing toxicity; all these effects thereby improve drug efficacy, safety and patient compliance.

Moreover, by finely engineering the NC shell architecture, one can add many other desirable features for a drug delivery system such as an on demand release of the payload and an ability to target a specific site.

Typical examples of delivery systems designed to improve the therapeutic index of poor water-soluble agents include liposomes, polymeric nanoparticles, solid lipid nanoparticles, and nanostructured lipid carriers.

There are several available strategies to produce biodegradable NCs such as nanoprecipitation, emulsion diffusion, coacervation [9, 10], co-crystallization

[11], formation of complexes such as cyclodextrins [12], and use of aqueous mixtures with an organic solvent [13].

However, all these approaches share some major limitations including safety issues and procedures leading to simple architectures that prevent a fine control and tuning of the shell properties [14]. Hence, combining degradable NCs along with a multifunctional and multicompartment architecture still remains challenging [15, 16].

In this context, lipid NCs based on oil in water (O/W) NE technology provide an avenue to address some major issues. Firstly, these drug nanocarrier systems appear to be way more biocompatible than their polymeric counterparts, which may contain residuals from cytotoxic monomers, catalysts and organic solvents. Moreover, even when compared to liposomes - which despite many others encapsulating systems are already used in some cancer therapies - lipid NCs apparently have an edge over them. Otherwise than liposomes, indeed, lipid NCs have a high lipophilic drug loading capacity, do not require the use of organic solvents and they do not suffer from a premature release of their payload [17].

True is that in order to achieve long term stability and use of (O/W) NEs as liquid templates for multilayer NCs, it is crucial to finely control both their size and polydispersity. In fact, these two features directly reflect on the NE shelf life.

From a thermodynamic point of view (O/W) NEs may be seen as liquid-liquid interfaces, which are highly dynamic and intrinsically unstable systems [18]. Basically, this is due to the immiscible nature of the oil and water phases and to the high interfacial tension, even when stabilized by surfactants. However, if one is able to take advantage of their elevated fluidity and tendency to reduce surface tension by interacting with adjacent molecules or nanoparticles, then it is possible to drive the assembly process in a unique

fashion [19]. Hence, (O/W) NEs show great potential as viable templates for ordered assembly of molecules and nanoparticles.

Some attempts have been already pursued in this direction by carrying the process of multiple polymer deposition at liquid-liquid interfaces based on O/W NEs but with little control over size and stability. This is especially relevant when multiple polymer depositions are required, as it is in the case of Layer-by-layer (LbL) multifunctional polymeric NCs [20-24].

LbL technique is recognized as one of the most promising methods to prepare engineered multifunctional NCs. It is based on the progressive deposition of polymer layers on a given template and it allows for control almost at the molecular scale [25-28]. The main driving force of the process is the electrostatic attraction between polyelectrolyte layers of opposite charge, which makes the deposition procedure relatively simple and straightforward [29]. However, in a typical protocol to obtain multilayer hollow capsules, the deposition of the polyelectrolyte-based shell is performed around a solid template, which eventually needs to be removed in order to leave an inner cavity acting as a reservoir. Due to the harsh conditions required for removing the template, several polymer layers are generally needed in order to strengthen the capsule and avoid damages. In addition, the large number of layers generally implies centrifugation and rinse steps, which in turn force to the use of dense templates hard to leach out [30]. For all these reasons, monodisperse hollow capsules are typically reported only in the case of sizes much larger than 200 nm or by use of strong synthetic polymers such as poly(allylamine hydrochloride) and poly(styrene sulfonate) [30]. Both conditions virtually dismiss the as prepared LbL capsules from an effective application as drug delivery systems [26, 31]. It is in this context that liquid templates sweep in as a viable way to overcome most of the limitations related to LbL around solid templates [31, 32]. Once the deposition of polyelectrolytes has been performed around a liquid drop it does not need to be removed, thus avoiding tedious and time consuming

post-processing and any constraint on the minimum number of layers [14]. Also, when using (O/W) NEs as liquid templates one can preload big amounts of lipophilic molecules – which are the most recurrent among therapeutic agents – by directly dissolving them into the oil phase [33-35].

From a safety point of view, the oil-core itself should not represent an issue in principle. Whereas, all the risks of template residues and damaging of the polymer shell due to harsh leaching out conditions should be wiped out by the use of liquid templates [14, 36].

In this panorama, optimized (O/W) NEs capable to sustain multiple LbL depositions of biodegradable polymers may provide an effective avenue for the delivery of lipophilic agents. This way, on the one hand, one can take advantage of the classical LbL technique, which has emerged as one of the easiest and most controlled methods to deposit ultrathin polymer layers [25]; on the other hand, (O/W) NEs provide a lipophilic liquid core which allows for high payloads of powerful lipophilic drugs [23, 28], sizes under 200 nm and naturally derived polymer shells.

Following this aim, we here report on the use of a liquid–liquid interface based on a O/W chitosan coated NE as a reliable template for multiple interfacial depositions of polymers to produce highly controllable polymer NCs [37]. Many efforts were devoted to redeem the limitations of the liquid core of LbL NCs in order to take advantage of their great potential as delivery systems. Through the development of new methodologies we produced ultrastable, highly concentrated (ca. 10 wt% oil phase), narrowly distributed NCs. Their morphological characteristics were highlighted by classical dynamic light scattering (DLS) combined with advanced analysis such as cryo transmission electron microscopy (cryo-TEM) and super resolution confocal microscopy (STED). Also, in order to assess the protection role of the polymer shell, we carried out biological tests comparing cell viability after incubation with NCs prepared with different number of layers around the liquid core.

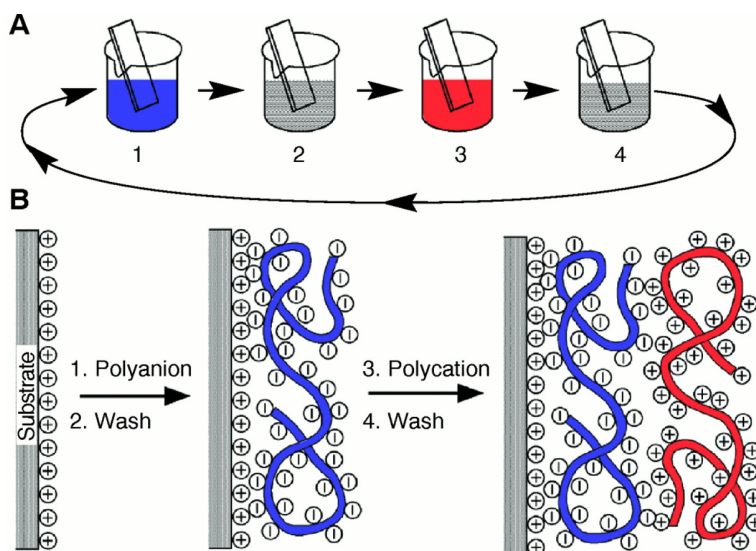


Figure 2.1.1 (A) Schematic of the film deposition process using slides and beakers. Steps 1 and 3 represent the adsorption of a polyanion and polycation, respectively, and steps 2 and 4 are washing steps. The four steps are the basic buildup sequence for the simplest film architecture, $(A/B)_n$. The construction of more complex film architectures requires only additional beakers and a different deposition sequence. (B) Simplified molecular picture of the first two adsorption steps, depicting film deposition starting with a positively charged substrate. Counterions are omitted for clarity. The polyanion conformation and layer interpenetration are an idealization of the surface charge reversal with each adsorption step. (Figure redrawn after ref. [29]).

2.2 Results and Discussion

Nanoemulsions are reliable liquid templates

The opportunity to use O/W NEs as reliable liquid templates for the preparation of polyelectrolytes multilayer NCs strongly depends on NE stability and dimensional features, such as average size and size distribution. However, NEs are thermodynamically unstable systems due to the immiscibility of the oil and water phases, even when stabilized by surfactants. At the same time, it is behind their intrinsic dynamic and unstable nature that their unique behavior hides. The elevated interfacial tension and fluidity, indeed, provide high mobility for the achievement of an equilibrium assembly [19], making NEs viable templates for Layer by Layer polymer NCs.

Moreover, the use of O/W NE based liquid templates allow for pre-loading of high amounts of lipophilic agents redeeming the subsequent built up of the polymer nanocapsule from a number of heavy constraints.

Hence, by addressing the stability and dimensional issues, one can benefit of all the unique properties of O/W NE as liquid templates for multilayer NCs.

In this work the typical limitations of liquid templates have been bypassed starting from nanomulsions stabilized by means of a polymer coating, namely secondary NEs, combined with an optimal re-dispersion process already described in a previous work [38].

Small sizes (under 200 nm) and low PDI of the oil template (<0.1) were achieved through high-pressure homogenization according to a procedure previously reported [38]. For what concerns the template size, we used two different formulations, namely L_{130} and L_{90} (based on different concentrations of surfactant in oil 2.4 g/20 g and 4.8 g/20 g, respectively). These primary NEs feature a reproducible size, ranging from around 130 nm (L_{130}) to around 90 nm (L_{90}). Then, we stabilized the primary nanomulsions through a polyelectrolyte

coating made of chitosan (CT), a biodegradable polysaccharide [39]. To prevent aggregation, the secondary NEs were properly re-dispersed according to the procedure previously reported [38]. We were therefore able to highly improve monodispersity along with the stability of the liquid templates, as schematically represented in the case of L_{90} secondary NE in **Figure 2.2.1b**.

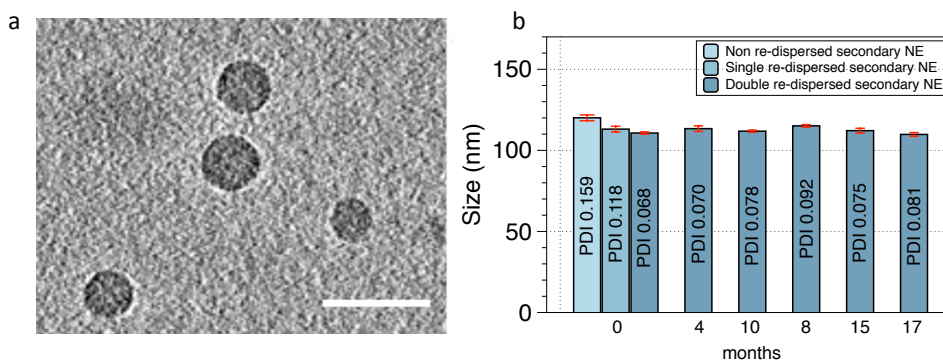


Figure 2.2.1 (a) cryo-TEM analysis of a double re-dispersed secondary NE sample after about six months from the preparation; (scale bar: 200 nm). (b) Size and PDI over time of double re-dispersed L_{90} based secondary NE at an oil concentration of 10 wt% (light blue). Comparison at 0 time among size and PDI values of double re-dispersed (light blue), single re-dispersed (medium blue) and non re-dispersed (dark blue) L_{90} based secondary NE.

As it emerges from the histograms in **Figure 2.2.1b**, performing twice the re-dispersion process after coating the NE with chitosan avoided aggregation, and kept secondary NE size similar to the starting size of the primary NEs when compared to non-re-dispersed and single re-dispersed systems. More interestingly, this procedure guaranteed more than one year of stability. The DLS measurements performed in order to monitor the size and PDI changes over time, were also supported by morphological analysis.

Still in **Figure 2.2.1a** we also reported the cryo-TEM of the double re-dispersed secondary NE after about six months of preparation, which seems to confirm the DLS data.

Further investigations about the dimensional features of our secondary NEs were performed by super resolution fluorescence microscopy. In particular, L_{130} and L_{90} secondary NEs (0.1 wt% polymer - 10 wt% oil) were analyzed using a confocal laser scanning microscope in stimulated emission depletion (STED) modality, because of their expected small size (**Figure 2.2.2a,c**).

For this purpose, chitosan was chemically labeled with Fluorescein 5(6)-isothiocyanate (FITC) before deposition. The results depicted in **Figure 2.2.2** seem in good agreement with the analysis carried out by DLS.

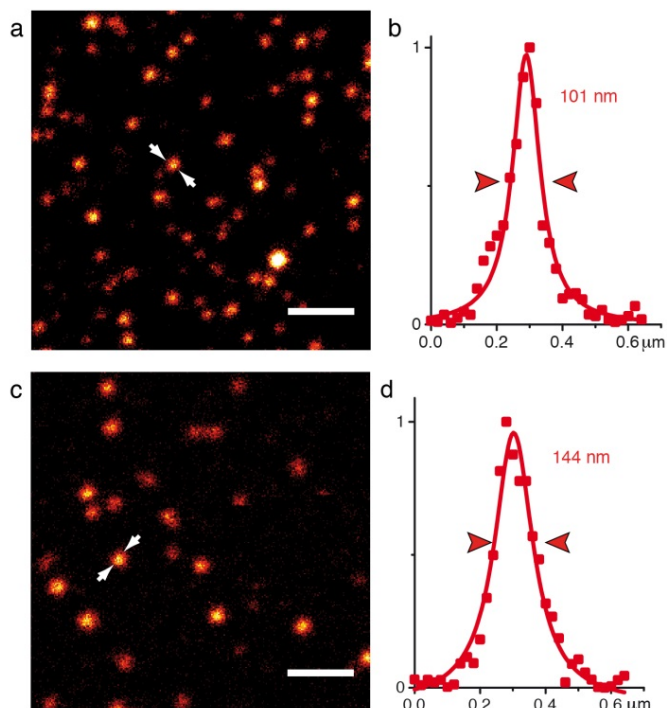


Figure 2.2.2 STED analysis of L_{130} and L_{90} secondary NEs and the corresponding line profile of the intensities comprised between the two arrows shown in (a), (c) respectively. The red dots depicted in panel b and d show the intensities of the corresponding pixel values in the image, red line is a Lorentian fit of the values. (Scale bar: 1 μm).

Multilayer deposition on oil-core nanocapsules

The LbL technique has emerged as one of the most promising methods to prepare engineered multifunctional NCs through the self-assembly of polyelectrolytes mainly driven by electrostatic interactions [25]. It is recognized as an easy and controlled technique to deposit ultrathin polymer layers around almost any kind of template. Nevertheless, only few attempts have been pursued to produce polyelectrolyte multilayer NCs starting from O/W NE based liquid templates [20-24]. As it was already discussed in the introduction to this chapter, this is also due to high reactivity of liquid-liquid interfaces, which can make the LbL deposition process difficult to handle.

However, thanks to the stabilization of the primary NE described in the previous paragraph and to a customized wash-less deposition method, we managed to finely perform LbL technique around nanosized liquid templates. In particular, we obtained narrowly distributed oil-core multilayer NCs starting from a 20% O/W NE. We were able to deposit up to seven polymer layers while keeping the size below 200 nm and the PDI below 0.1. In order to preserve these dimensional features during deposition of several polymer layers onto highly concentrated secondary NEs (10 wt%), the LbL process was aided by a sonication step in a water bath at controlled temperature. In addition, to keep a good control on the mixing step, polymer solution, and NE template were injected and mixed drop wise. A scheme of this set-up is depicted in **Figure 2.1**. Finally, we identified by saturation method the optimal polymer amount to deposit at each step of the LbL procedure as reported in **Figure S1** in the Supplementary Information section.

The results of these depositions are summarized in **Figure 2.2.3** and **2.2.4** (see also Figure S2 in the Supporting Information). The cryo-TEM analysis clearly shows the different size between the L_{90} based pentalayer (**Figure 2.2.3a**) and L_{130} based eptalayer (**Figure 2.2.3d**) confirming the size distribution

observed by DLS. Moreover, both the penta- and the eptalayer NCs, imaged in their frozen hydrated state, appeared to be formed by a dense core, corresponding to the oil template, surrounded by a well-defined electron-dense boundary.

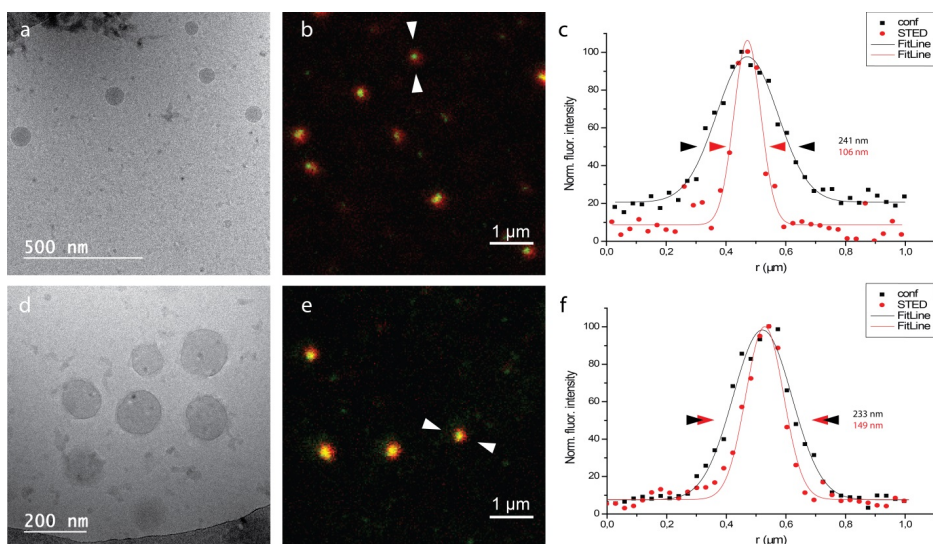


Figure 2.2.3 (a), (d), Cryo-TEM projection images of L_{90} based pentalayer and L_{130} based eptalayer NCs, respectively. Panels (b) and (e) are an overlay of a STED acquisition of the FITC-chitosan (last layer, green), and a confocal acquisition of TRITC-chitosan (underlying layer, red). Panels (c) and (f) are the line profiles of the FITC fluorescence intensities comprised between the two arrows shown in (b) and (e), respectively. Red dots show the intensities of the corresponding pixel values in (b) and (e), while red line is a Gaussian fit of the values.

We also characterized the size and distribution of our multilayer NCs, by STED analysis of both the L_{90} based pentalayer (**Figure 2.2.3b**) and L_{130} based eptalayer (**Figure 2.2.3e**). To this purpose, we labeled the last chitosan layer with FITC, while the second to last chitosan layer was stained with Rhodamine B isothiocyanate (TRITC) fluorophore to analyze the co-localization between them. In agreement with the DLS measurements, we proved by STED the narrow distribution feature of the developed NCs on both sizes (**Figure 2.2.3b,c,e,f**); while the perfect matching between green and red colors (FITC and TRITC respectively) proves the effectiveness of the deposition

homogeneity. This analysis is a further evidence of the effective LbL deposition of each layer since only the last one was labeled with FITC.

We then proved the loading capability of the NCs to be effective by dissolving inside the oily templates lipophilic model drugs like Nile Red (**Figure 2.2.4e**) and curcumin, (**Figure 2.2.4f**), without affecting NCs size, PDI and templating capability.

Another appealing feature of our liquid templates is their capability to undergo a multilayer deposition even after storing the secondary NE for more than one year. Such stability is reported in **Figure 2.2.4f** that depicts the LbL process in terms of size, PDI and Z-potential of a pentalayer prepared on a L_{90} template loaded with curcumin stored for 14 months.

In this study, we also showed the versatility of the method by testing other couples of polyelectrolytes (i.e. chitosan-sodium alginate, chitosan-hyaluronic acid) and the results of size, PDI and Z-potential are summarized in **Figure 2.2.4c**, **2.2.4d** and **Table S2c**, **S2d** in the Supplementary section.

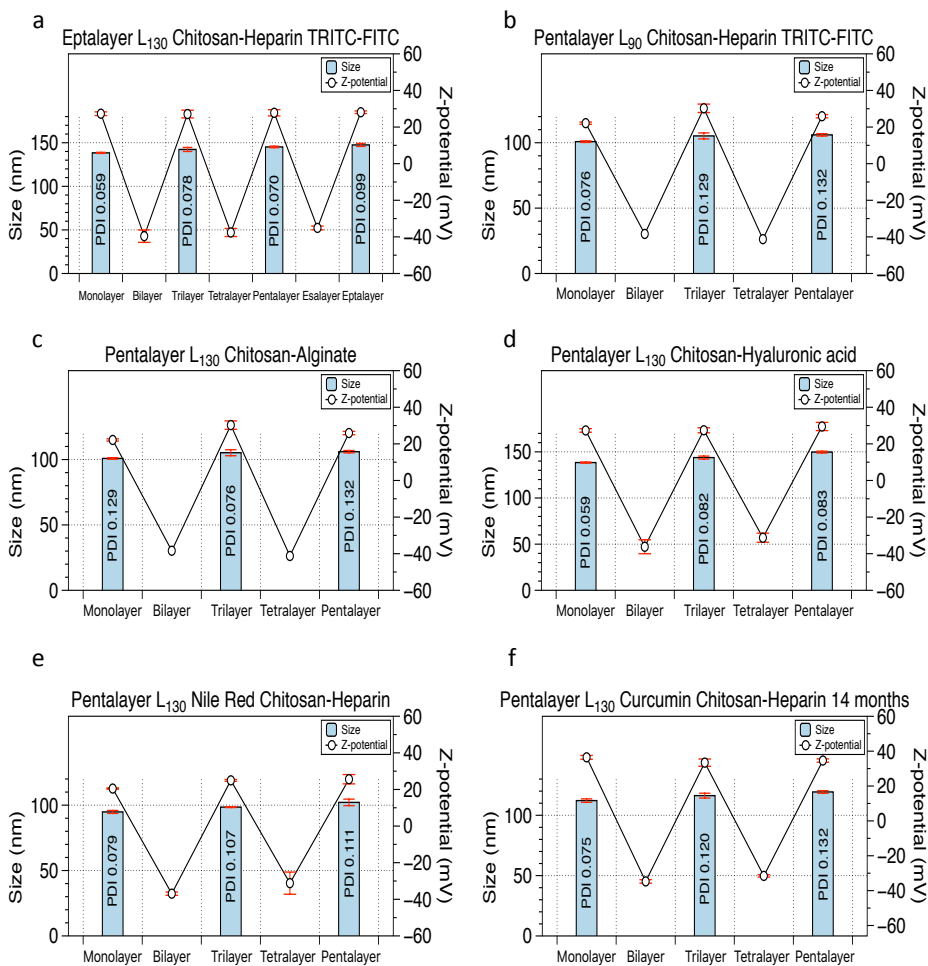


Figure 2.2.4 Overlay of size increase and potential reversal, by DLS, showing the versatility of the deposition process in terms of fluorophores labeling (a), (b) variety of biocompatible polyelectrolytes (c), (d), loading capability of model drugs (e) and possibility to perform LbL deposition using 14 months old templates (f).

Nanocapsules number of layers affects their biological applications

To understand how the number of layers can affect the final biological application of our NCs we carried out a biological analysis testing L_{90} based systems. In particular, we compared a monolayer, a trilayer, and a pentalayer in order to keep the same chemical interface corresponding to chitosan in all the three cases. The starting NE was loaded with curcumin, which is hydrophobic as most of the nutraceuticals and has already demonstrated anticancer effects [40]. The three nanocapsular systems were put in contact with human colon cancer cell line (HT29) for 72 h; the results of the viability tests are shown in **Figure 2.2.5a**. The monolayer resulted more toxic than the trilayer and even more than the pentalayer at all times and concentrations tested. In particular, at the maximum concentration of curcumin (30 $\mu\text{g/ml}$), the monolayer reached the IC_{50} in 24 h, while the trilayer did it in 48–72 h and the pentalayer in 72 h. The time point at 72 h was sufficient for the monolayer to reduce the viability to very low values (almost 10%). In order to exclude that the difference of toxicity could be due to a different amount of internalized nanoparticles, we also carried out an internalization test of the three systems in the first 24 h, which showed no significant difference (**Figure 2.2.5b**). As expected, from this study it is clear that the number of layers has an impact on the final biological application confirming the protective function of the multilayer, especially when switching from the monolayer to the trilayer system. This feature is less pronounced when passing from the trilayer to the pentalayer. In addition to this consideration, it is valuable to remark the capability of a completely biosafe nanocarrier to be active against cancer cells thus enabling the administration of a potential cancer therapy with no side effects.

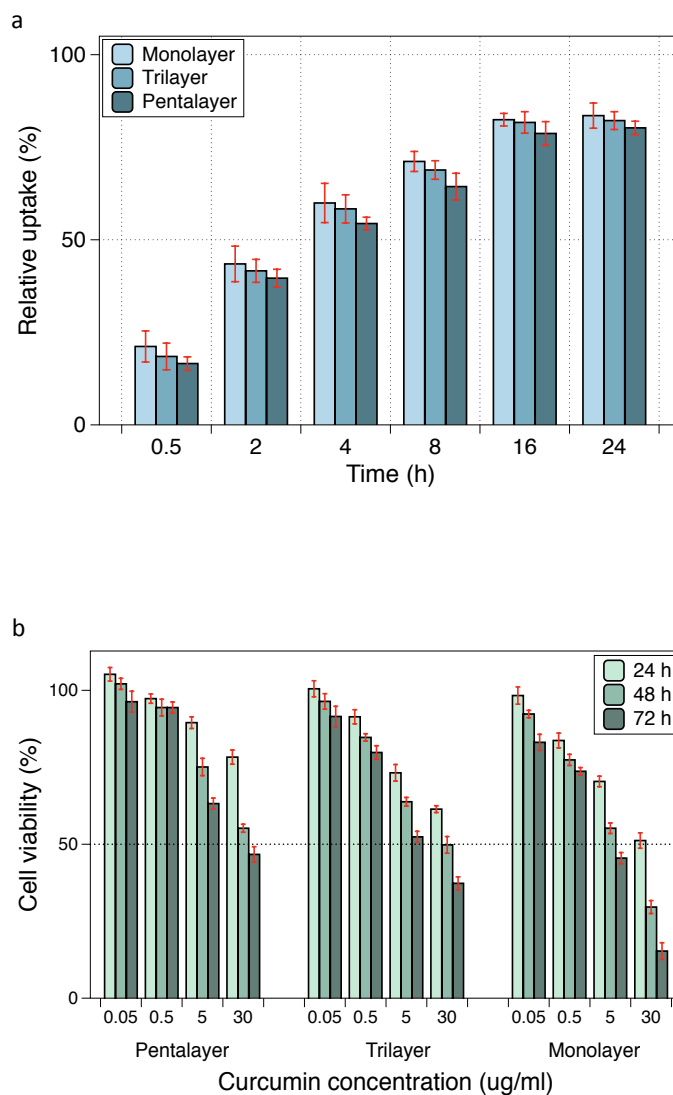


Figure 2.2.5 Cell uptake (a) and viability (b) study on HT29 cells after incubation with monolayer trilayer and pentalayer NCs.

2.3 Conclusions

The main goal of this research work was trying to redeem some of the limitations of liquid templates in the built up of polymer multilayer NCs, in order to take advantage of their unique properties.

Based on the results obtained, in this work we propose a viable route that allows the use of a food grade NE stable enough to build up dimensionally controllable natural polymer multilayer NCs. These systems are of huge interest for nanomedicine.

The liquid cores of the proposed NCs have a narrowly distributed size well under 200 nm, which has been achieved through an in-house consolidated method. Moreover, they show long-term stability, which effectively extends their shelf life and increases their application potential. These properties combined with an improved LbL procedure allowed for deposition of polymer layers directly at a liquid-liquid interface that is generally prevented by the instability of such liquid templates. This result provides a possible alternative to the LbL onto solid core templates.

In order to add some other interesting features, efforts were devoted to increase the oil-core concentration during the LbL deposition of the multilayer NCs while preserving the dimensional properties. A 10% oil phase was welcome as a fulfilling compromise, also when compared to literature. Moreover, the polymer deposition method proved to be flexible by use of different kind of naturally derived polyelectrolytes such as hyaluronic acid, and sodium alginate.

To highlight the advantage of pre-loading the NCs with relatively high amounts of lipophilic agents, we embedded curcumin in the oil-core without any post processing after multilayer deposition around the liquid template. These ready to use NCs demonstrated to be active against the human colon cancer cell line with a tunable time of action depending on the number of layers.

In conclusion, here we propose a reliable method to prepare robust and versatile lipid nanocarriers taking advantage of both liquid templates and LbL techniques. This stays still a relatively basic version of NCs, though. Many other appealing properties, such as multifunctional performance or on demand release of the payload, can be added to the NCs to increase their potential. Thanks to their multicompartment architecture, the possibility to finely engineer their polymer shell and to embed a number different molecules - which is limited only by one's imagination - we believe that oil-core LbL NCs provide an avenue for the production of effective delivery systems in nanomedicine.

2.4 Materials and Methods

Materials

O/W NEs were prepared using Soybean oil (density at 20 °C of 0.922 g/ml) and surfactant Lipoid E80 (egg lecithin powder 80-85% enriched with Phosphatidyl choline (PC) and 7-9.5% content in phosphatidyl ethanolamine (PE)) purchased from Lipoid and used without further purification. Millipore® Milli-Q water was used for the preparation of all NEs and solutions. Chitosan (CT, LMW 90-150 kDa, DDA 84% determined via ¹H-NMR) and heparin sodium salt from porcine intestinal mucosa (17-19 kDa), sodium alginate were purchased from Sigma Aldrich.

Fluorescence imaging of multilayer NCs was performed tagging some chitosan layers with fluorophores, specifically with Fluorescein isothiocyanate (FITC) (m.w. = 389.38 g/mol) and Rhodamine B isothiocyanate TRITC (m.w. = 536.08 g/mol), both of them purchased from Sigma Aldrich and used without further purification.

Additional polyelectrolytes such as hyaluronic acid and was kindly supplied by Istituto Nazionale Tumori - IRCCS "Fondazione G.Pascale" and used to enrich the polymer shell of multilayer NCs.

The loading capability of the NCs was assessed by dissolving lipophilic model drugs such as Nile Red and Curcumin from Curcuma longa (Turmeric) powder (m.w. = 368.38 g/mol) purchased from Sigma-Aldrich and used with no further purification.

Nanoemulsion template preparation

NEs were prepared according to a two-step procedure previously developed [38]. First, a pre-emulsion and re-dispersion step is needed to achieve nanosized

and monodispersed O/W emulsions. While in a second step the narrowly distributed NE is coated with a positively charged chitosan layer, which contributes to significantly extend the stability of the system over time. This chitosan-coated NE has been named secondary NE.

Briefly, in the first step the surfactant Lipoid E 80, and any possible lipophilic payload, is dissolved in a weighed amount of soybean oil under magnetic agitation until a homogeneous oil phase is observed. Then, the oil phase is added dropwise to a weighted amount of aqueous phase (Milli-Q water) and the two are mixed up with an immersion sonicator. This mixing process lead to a roughly dispersed O/W emulsion where the oil drops size is around 500 nm. The emulsion is finally passed at 2000 bar through a high-pressure valve homogenizer (Microfluidics M110PS) for first three individual cycles - to strongly reduce the initial size - and then by re-filling the reservoir for 200 steps. This method was used for the preparation of 20 wt% O/W NEs. Two different concentrations of lecithin in oil were used in this study, namely 0.12, 0.24 (w/w), respectively labeled L_{90} and L_{130} .

Then, 0.1 M acetic acid solution of chitosan (0.125 wt%) was prepared and brought to pH 4 with the addition of NaOH. Each NE (L_{90} , L_{130}) 20 wt% oil phase was added to the chitosan solution quickly under vigorous stirring and kept under stirring for 15 min to allow uniform chitosan deposition. Final concentrations of oil and chitosan were 10 wt% and 0.1 wt%, respectively, while the pH of the final secondary nano-emulsions was 4. These NEs were properly re-dispersed by using the method reported in the previous work [38], stored at room temperature and analyzed over time.

Polyelectrolytes multilayer deposition

The previously described NE represents the oil template in the core-shell architecture of our NCs. We then grew a polymer shell around the liquid core to

enrich the NCs with further functionalities. To this aim we took advantage of the versatility of the layer-by-layer technique. According to this method, the multilayer structure was built up alternating polyelectrolyte layers of some negatively charged polymers (such as heparin, sodium alginate and hyaluronic acid) with the positively charged chitosan. The sequential deposition of the oppositely charged polymers led to the formation of eptalayer capsules in the case of L_{130} template and pentalayer capsules for L_{90} .

In order to highlight the multilayer structure of the NCs and provide a proof of concept of the deposition process, the last two chitosan layers of both eptalayer (L_{130} based) and pentalayer (L_{90} based) were labeled respectively with Rhodamine (TRITC) and Fluorescein (FITC).

In order to prepare highly concentrated multilayer with a narrow size distribution, we developed a new methodology allowing for a higher control over the deposition process. Experimentally, the eptalayer and pentalayer NCs were prepared by aid of two syringe pumps (HARVARD APPARATUS 11 PLUS) and an ultrasonic bath (FALC INSTRUMENTS). Starting from the chitosan coated NE (10 wt% oil and 0.1 wt% chitosan), a negatively charged second polymer layer was deposited by mixing 1:1 (v:v) of a 0.175 wt% aqueous solution of heparin with the NE suspension. The two liquid phases were injected at the same flow rate (0.4 ml min^{-1}) through two micrometric capillaries interfaced at their extremities. Each drop was then collected inside a glass tube immersed in the ultrasonic bath at room temperature, 59 kHz and 100% power. The same procedure was repeated also for the deposition of the subsequent polyelectrolyte layers according to the following concentration ratios: chitosan/heparin = 2.25 for the odd number layers and heparin/chitosan = 1.75 for the even number layers.

Particle size and Z-potential characterization

Size distribution and Z-potential of all the suspensions were measured by using the Dynamic Light Scattering (DLS) ($\lambda = 632.8$ nm) and particle electrophoresis techniques, respectively (Zetasizer NanoSeries, Malver).

All the suspensions were diluted to a droplet concentration of approximately 0.025 (wt%), using Milli-Q water in the case of NEs and multilayers ending with heparin. While the NCs ending with a chitosan layer were diluted in acetic acid Milli-Q water solution (pH 4; 20 mM).

Z-potential measurements were performed to get indications about colloidal dispersion stability of all the suspensions. Also, it was a key method to follow the layer-by-layer procedure in building up of the polymer shell of the NCs. The successful deposition of each polymer layer was indeed confirmed by the potential reversal due to the alternation of polyelectrolytes of opposite charge. Furthermore, through Z-potential measurements it was also determined the proper amount of polyelectrolytes for each deposition step, which fully covers the surface of the NCs without exceeding in the dispersant phase.

The Z-potential of all the suspensions was determined using a particle electrophoresis technique where the direction and velocity of droplet movement in a well defined electric field is monitored. Prior to analysis, all the suspensions were diluted in the same conditions as it was for the size measurement.

Cryo-TEM characterization of the system

The morphology of the NEs and multilayer NCs were observed by cryo-TEM. In particular, frozen hydrated samples were prepared by applying a 3 μ l aliquot to a previously glow-discharged 200 mesh holey carbon grid (Ted Pella, USA). Before plunging into nitrogen cooled liquid ethane, the grid was blotted for 1.5 s in a chamber at 4 °C and 90% humidity using a FEI Vitrobot Mark IV

(FEI company, the Netherlands). The particles were imaged using a Tecnai G2 F20 transmission electron microscope (FEI company, the Netherlands) equipped with a Shotky field emission gun operating at an acceleration voltage of 200 kV and recorded at low dose with a 2k x 2k Ultrascan (Gatan, USA) CCD camera.

STED analysis of nanocapsules

NC size was also measured using super-resolution microscopy, i.e. stimulated emission depletion (STED). In order to preserve as much as possible the shape and the polydispersion of the NCs, we developed a procedure to prepare the samples for imaging with STED nanoscopy. Each sample was diluted (a 1:50 dilution was chosen for the monolayers and a 1:12.5 dilution for the trilayers in order to have the same oil concentration of 0.02 wt%) in a heppendorf with a 20 mM acetic acid buffer solution at pH 4 and was put in a FD3510 fluoro dish for 30 min to allow it to adhere to the surface of the dish. After that, 3 washes with a 5 wt% dabco antifade solution were performed and at the end the central part of the dish was left full of dabco during sample observation. In particular dabco antifade was needed to avoid the bleaching effect of the FITC-labeled chitosan. Samples were imaged by means of a Leica TCS STED-CW microscope (Leica-Microsystems, Mannheim, Germany). The resolution of the microscope was estimated to be < 80 nm. For each different sample, we acquired 10 images with a field of view of $25.6 \times 25.6 \mu\text{m}$ for a pixel size of 25×25 nm. The STED-CW beam power was 430 mW, measured at objective back focal plane. The image analysis was carried out by ImageJ software [41].

Moreover, a STED analysis was also crucial to provide a further demonstration of the multilayer structure of the NCs polymer shell and of its tunability. This was achieved by a STED acquisition of the FITC-chitosan (last layer), and a confocal acquisition of TRITC-chitosan (underlying layer).

Cytotoxicity assay

Human colon cancer cells 1 (HT29 ATCC®) were seeded in a 96-well plates at a density of 3000 cells/well), cultured in Dulbecco's Modified Eagle's Medium and McCoy's 5A medium (Sigma Aldrich, Milan, Italy) supplemented with 2 mM Glutamine (Gibco® Life Technologies, Monza, Italy), 10% Fetal Bovine Serum (FBS) (Gibco® Life Technologies, Monza, Italy) and 1% Penicillin Streptomycin (Gibco® Life Technologies, Monza, Italy). Cells were then incubated for 24 h under standard conditions (5% CO₂, 100% humidity, 37 °C).

The cytotoxicity of the formulations (monolayer, trilayer, pentalayer) was assessed on human colon cancer cells (HT29) by evaluating the activity of the mitochondrial dehydrogenase by of a modified MTT [3-(4,5-dimethylazol-2-yl)-2,5 diphenyltetrazolium bromide] method according to the manufacturer's instructions (Dojindo Molecular Technologies Inc., Rockville, MD). Human colon cancer cells were seeded in 96-well plates at a density of 10000 cells per well in complete medium at 37 °C in a humidified 5% CO₂ atmosphere. For all the formulations, we performed time-course (from 24 up to 72 h) and dose-response experiments (from 0.05 up to 30 µg/ml of curcumin). At the end of the incubation cells were washed three times with PBS (pH 7.4) and incubated with 100 µl of a MTT solution (0.5 mg/ml in cell culture medium) for 4 h. The absorbance was acquired at a wavelength of 450 nm with a Tecan Infinite M200 plate-reader using I-control software. The relative cell viability (%) was calculated by the formula $[A]_{\text{test}}/[A]_{\text{control}} \times 100$, where “[A]test” is the absorbance of the test sample, and “[A]control” is the absorbance of the control cells incubated solely with culture medium. After the evaluation of cell cytotoxicity, we measured the total protein content by using the Micro BCA protein assay kit (Pierce). Briefly, cells were washed with ice-cold PBS, and incubated for 15 min in 150 µl cell lysing buffer (0.5% v/v Triton X-100 in

PBS), supplemented with 150 μl of Micro BCA protein assay kit reagent (prepared following the instructions of the manufacturer). Finally absorbance was measured at 562 nm with a plate reader. Cytotoxicity measurements were then normalized by the amount of total protein content in each well.

Cell uptake analysis

For uptake experiments HT29 cells were seeded in a 24-well plate at a density of 5×10^3 cells/well and allowed to grow for 24 h. The medium was then replaced with 500 μl of solution containing monolayer, trilayer and pentalayer with an equivalent curcumin molar concentration of 2.71 μM suspended in culture medium. Cells were then incubated for a time comprised between 0.5 and 24 h. Cells were then washed twice with PBS (pH 7.4), at the end of the experiments the supernatant was removed and the cells were washed three times with 10 mM PBS. Afterwards cells were lysed with 0.1 ml of 0.5% Triton X-100 in 0.2 N NaOH. The membrane-bound and internalized NEs were quantified by analyzing the fluorescence of the cell lysate ($\lambda_{\text{exc}} = 420$ nm, $\lambda_{\text{em}} = 550$ nm). Calibration was performed for each formulation dispersing the nanocapules with a curcumin concentration of 10 μM up to 0.2 nM in a cell lysate solution (10^6 untreated cells dissolved in 1 ml of the Triton X-100/0.2 N NaOH solution).

2.5 Supplementary Section

Saturation method

For both the bilayer and the trilayer the optimal concentration of polymer to fully cover the NCs without exceeding was determined by saturation method. This methodology offers the great advantage to avoid post-processing procedures such as centrifuge and washing steps which typically follow the LbL deposition. Experimentally, the ratio between the concentrations of the polymer to deposit and the polymer already covering the NCs was increased until the Z-potential of the suspension reached a plateau. In particular, the two graphs in **Figures S1** show how for small ratios the amount of polymer added to the suspension only allows for a partial coating of the NCs which basically keep their initial surface charge. For example in **Figures S1a**, when the concentration of heparin employed to form a bilayer is only 0.5 folds higher than the concentration of chitosan coating the starting monolayer suspension, the Z-potential of the monolayer just undergoes a slight decrease. Whereas, for higher ratios we observe the switch of the Z-potential from the positive values of the monolayer to the negative ones due to the formation of a heparin bilayer. Then, the ideal value of concentration of polymer to add is considered to be the first point of the plateau region.

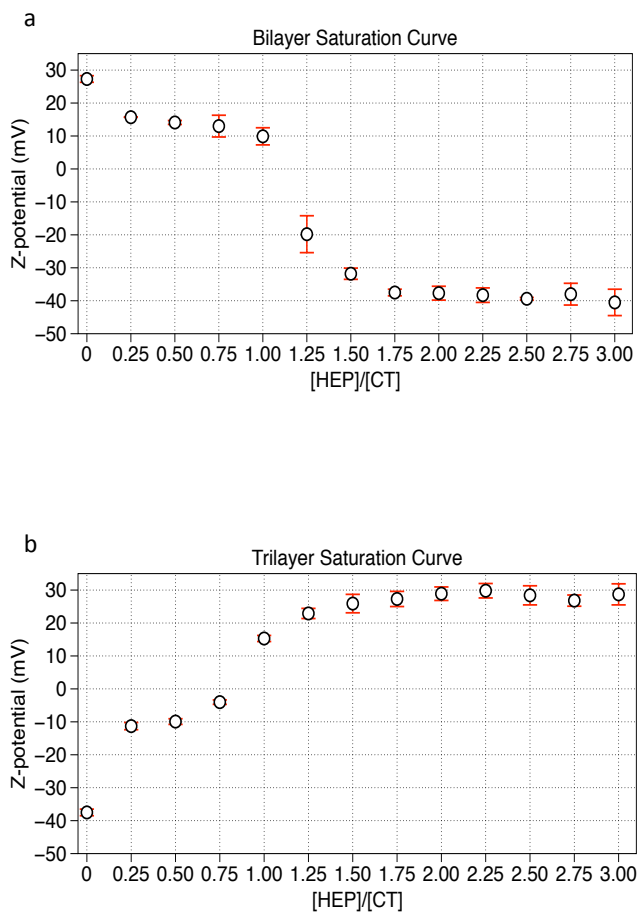
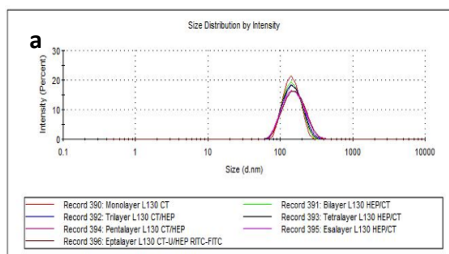


Figure S1 Identification of the optimal concentration ratio of two consecutive oppositely charged polyelectrolyte layers by DLS.

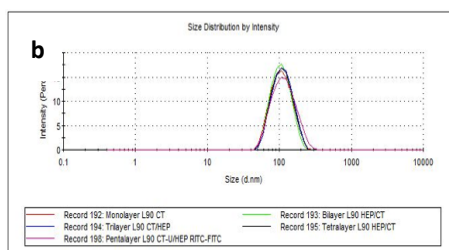
Zetasizer analysis of multilayer nanocapsules

Primary NEs obtained according to the method reported in the Method section were characterized by DLS in terms of average size, polydispersity index and Z-potential. The results are summarized in Figure S2.

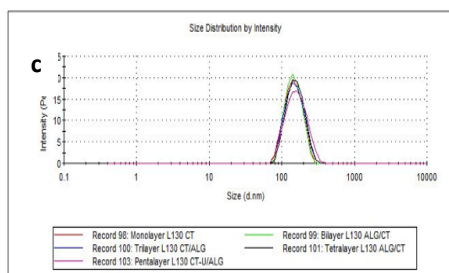
| Sample | Average size (nm) | st.dev | PDI | Z-potential (mV) | st-dev |
|------------|-------------------|--------|-------|------------------|--------|
| Monolayer | 138.4 | 0.6 | 0.059 | 27.3 | 1.0 |
| Bilayer | 138.6 | 0.7 | 0.059 | -39.6 | 3.4 |
| Trilayer | 142.3 | 2.3 | 0.078 | 27.1 | 2.1 |
| Tetralayer | 139.2 | 1.0 | 0.070 | -37.6 | 2.2 |
| Pentalayer | 145.2 | 0.9 | 0.095 | 27.8 | 1.7 |
| Esalayer | 142.6 | 0.7 | 0.093 | -35.2 | 1.1 |
| Eptalayer | 147.5 | 1.7 | 0.099 | 28.1 | 0.7 |



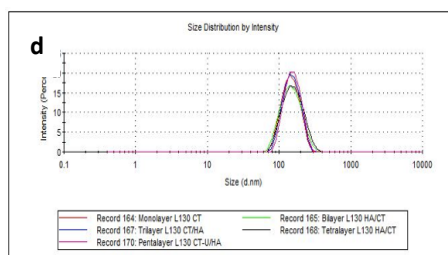
| Sample | Average size (nm) | st.dev | PDI | Z-potential (mV) | st-dev |
|------------|-------------------|--------|-------|------------------|--------|
| Monolayer | 100.9 | 2.2 | 0.076 | 22.1 | 0.5 |
| Bilayer | 99.7 | 0.6 | 0.103 | -38.4 | 4.6 |
| Trilayer | 105.2 | 3.3 | 0.129 | 30.2 | 1.1 |
| Tetralayer | 101.3 | 0.8 | 0.107 | -41.2 | 3.8 |
| Pentalayer | 106.0 | 1.5 | 0.132 | 25.9 | 1.2 |



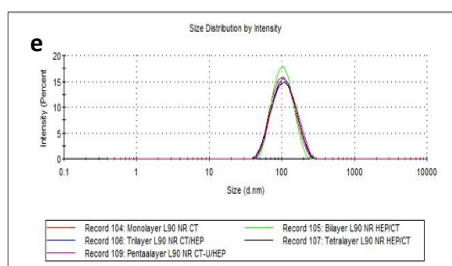
| Sample | Average size (nm) | st.dev | PDI | Z-potential (mV) | st-dev |
|------------|-------------------|--------|-------|------------------|--------|
| Monolayer | 138.4 | 0.6 | 0.059 | 27.33 | 1.0 |
| Bilayer | 141.6 | 1.2 | 0.091 | -44.30 | 4.6 |
| Trilayer | 144.7 | 2.5 | 0.086 | 28.38 | 3.6 |
| Tetralayer | 148.2 | 5.0 | 0.110 | -40.30 | 1.4 |
| Pentalayer | 150.4 | 4.1 | 0.097 | 26.08 | 1.0 |



| Sample | Average size (nm) | st.dev | PDI | Z-potential (mV) | st-dev |
|------------|-------------------|--------|-------|------------------|--------|
| Monolayer | 138.4 | 0.6 | 0.059 | 27.33 | 1.0 |
| Bilayer | 140.1 | 1.0 | 0.078 | -36.21 | 3.8 |
| Trilayer | 143.8 | 1.6 | 0.082 | 27.43 | 1.4 |
| Tetralayer | 148.8 | 0.3 | 0.085 | -31.27 | 2.5 |
| Pentalayer | 149.8 | 1.0 | 0.083 | 29.49 | 2.2 |



| Sample | Average size (nm) | st.dev | PDI | Z-potential (mV) | st-dev |
|------------|-------------------|--------|-------|------------------|--------|
| Monolayer | 98.9 | 1.6 | 0.091 | 18.5 | 1.3 |
| Bilayer | 97.6 | 0.8 | 0.093 | -37.0 | 1.3 |
| Trilayer | 100.5 | 0.7 | 0.113 | 25.3 | 2.5 |
| Tetralayer | 99.1 | 0.2 | 0.113 | -33.4 | 3.9 |
| Pentalayer | 103.5 | 1.4 | 0.119 | 24.7 | 2.4 |



| Sample | Average size (nm) | st.dev | PDI | Z-potential (mV) | st-dev |
|------------|-------------------|--------|-------|------------------|--------|
| Monolayer | 112.2 | 1.4 | 0.075 | 36.5 | 1.1 |
| Bilayer | 112.2 | 1.1 | 0.096 | -34.7 | 1.0 |
| Trilayer | 116.3 | 2.0 | 0.120 | 33.4 | 2.1 |
| Tetralayer | 109.7 | 1.1 | 0.106 | -31.5 | 0.7 |
| Pentalayer | 119.3 | 1.1 | 0.132 | 34.6 | 1.0 |

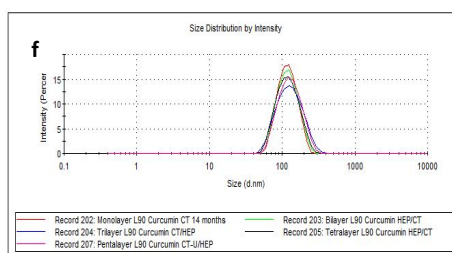


Figure S2 Average size, PDI, Z-Potential and size distribution of (a) FITC/TRITC eptalayer L_{130} chitosan/heparin (b) FITC/TRITC pentalayer L_{90} chitosan/heparin, (c) pentalayer L_{130} chitosan/alginate, (d) pentalayer L_{130} chitosan/hyaluronic acid, (e) pentalayer L_{90} chitosan/heparin loading NileRed, (f) pentalayer L_{90} chitosan/heparin loading curcumin.

Stability over time of multilayer nanocapsules

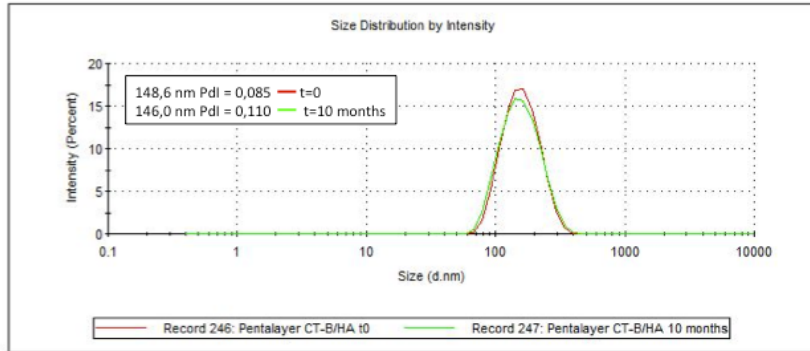


Figure S3 Chitosan-hyaluronic acid pentalayer size (D_H) stability over 10 months by DLS

2.6 References

- [1] Y. Yan, C.J. Ochs, G.K. Such, J.K. Heath, E.C. Nice, F. Caruso, Bypassing multidrug resistance in cancer cells with biodegradable polymer capsules, *Adv Mater* 22(47) (2010) 5398-403.
- [2] A. Zanotto-Filho, K. Coradini, E. Braganhol, R. Schroder, C.M. de Oliveira, A. Simoes-Pires, A.M. Battastini, A.R. Pohlmann, S.S. Guterres, C.M. Forcelini, R.C. Beck, J.C. Moreira, Curcumin-loaded lipid-core nanocapsules as a strategy to improve pharmacological efficacy of curcumin in glioma treatment, *European journal of pharmaceutics and biopharmaceutics : official journal of Arbeitsgemeinschaft fur Pharmazeutische Verfahrenstechnik e.V* 83(2) (2013) 156-67.
- [3] Y. Shen, E. Jin, B. Zhang, C.J. Murphy, M. Sui, J. Zhao, J. Wang, J. Tang, M. Fan, E. Van Kirk, W.J. Murdoch, Prodrugs forming high drug loading multifunctional nanocapsules for intracellular cancer drug delivery, *J Am Chem Soc* 132(12) (2010) 4259-65.
- [4] P. Lertsutthiwong, P. Rojsitthisak, Chitosan-alginate nanocapsules for encapsulation of turmeric oil, *Pharmazie* 66(12) (2011) 911-5.
- [5] R. Alvarez-Roman, G. Barre, R.H. Guy, H. Fessi, Biodegradable polymer nanocapsules containing a sunscreen agent: preparation and photoprotection, *European journal of pharmaceutics and biopharmaceutics : official journal of Arbeitsgemeinschaft fur Pharmazeutische Verfahrenstechnik e.V* 52(2) (2001) 191-5.
- [6] S. Stegemann, F. Leveiller, D. Franchi, H. de Jong, H. Linden, When poor solubility becomes an issue: from early stage to proof of concept, *European journal of pharmaceutical sciences : official journal of the European Federation for Pharmaceutical Sciences* 31(5) (2007) 249-61.
- [7] O.M. Koo, I. Rubinstein, H. Onyuksel, Role of nanotechnology in targeted drug delivery and imaging: a concise review, *Nanomedicine* 1(3) (2005) 193-212.
- [8] S.B. Lim, I. Rubinstein, R.T. Sadikot, J.E. Artwohl, H. Onyuksel, A novel peptide nanomedicine against acute lung injury: GLP-1 in phospholipid micelles, *Pharm Res* 28(3) (2011) 662-72.
- [9] C.E. Mora-Huertas, H. Fessi, A. Elaissari, Polymer-based nanocapsules for drug delivery, *Int J Pharm* 385(1-2) (2010) 113-42.
- [10] I. Youm, X.Y. Yang, J.B. Murowchick, B.B. Youan, Encapsulation of docetaxel in oily core polyester nanocapsules intended for breast cancer therapy, *Nanoscale Res Lett* 6(1) (2011) 630.
- [11] K. Shiraki, N. Takata, R. Takano, Y. Hayashi, K. Terada, Dissolution improvement and the mechanism of the improvement from cocrystallization of poorly water-soluble compounds, *Pharm Res* 25(11) (2008) 2581-92.
- [12] G. Tiwari, R. Tiwari, A.K. Rai, Cyclodextrins in delivery systems: Applications, *J Pharm Bioallied Sci* 2(2) (2010) 72-9.

- [13] A. Jouyban, Prediction of the optimized solvent composition for solubilization of drugs in water-cosolvent mixtures, *Pharmazie* 62(3) (2007) 190-8.
- [14] D.O. Grigoriev, T. Bukreeva, H. Mohwald, D.G. Shchukin, New method for fabrication of loaded micro- and nanocontainers: emulsion encapsulation by polyelectrolyte layer-by-layer deposition on the liquid core, *Langmuir : the ACS journal of surfaces and colloids* 24(3) (2008) 999-1004.
- [15] M. Delcea, A. Yashchenok, K. Videnova, O. Kreft, H. Mohwald, A.G. Skirtach, Multicompartmental micro- and nanocapsules: hierarchy and applications in biosciences, *Macromol Biosci* 10(5) (2010) 465-74.
- [16] S.H. Hu, S.Y. Chen, X. Gao, Multifunctional nanocapsules for simultaneous encapsulation of hydrophilic and hydrophobic compounds and on-demand release, *ACS Nano* 6(3) (2012) 2558-65.
- [17] N.T. Huynh, C. Passirani, P. Saulnier, J.P. Benoit, Lipid nanocapsules: a new platform for nanomedicine, *Int J Pharm* 379(2) (2009) 201-9.
- [18] K. Rahn-Chique, A.M. Puertas, M.S. Romero-Cano, C. Rojas, G. Urbina-Villalba, Nanoemulsion stability: experimental evaluation of the flocculation rate from turbidity measurements, *Advances in colloid and interface science* 178 (2012) 1-20.
- [19] Y. Lin, H. Skaff, T. Emrick, A.D. Dinsmore, T.P. Russell, Nanoparticle assembly and transport at liquid-liquid interfaces, *Science (New York, N.Y.)* 299(5604) (2003) 226-9.
- [20] S. Abbas, E. Karangwa, M. Bashari, K. Hayat, X. Hong, H.R. Sharif, X. Zhang, Fabrication of polymeric nanocapsules from curcumin-loaded nanoemulsion templates by self-assembly, *Ultrason Sonochem* 23 (2015) 81-92.
- [21] D.K. Beaman, E.J. Robertson, G.L. Richmond, Unique assembly of charged polymers at the oil-water interface, *Langmuir : the ACS journal of surfaces and colloids* 27(6) (2011) 2104-6.
- [22] Y. Li, M. Hu, Y. Du, D.J. McClements, Controlling lipid nanoemulsion digestion using nanolaminated biopolymer coatings, *J Microencapsul* 28(3) (2011) 166-75.
- [23] C. Preetz, A. Rube, I. Reiche, G. Hause, K. Mader, Preparation and characterization of biocompatible oil-loaded polyelectrolyte nanocapsules, *Nanomedicine* 4(2) (2008) 106-14.
- [24] K. Szczepanowicz, D. Dronka-Gora, G. Para, P. Warszynski, Encapsulation of liquid cores by layer-by-layer adsorption of polyelectrolytes, *J Microencapsul* 27(3) (2010) 198-204.
- [25] S. De Koker, R. Hoogenboom, B.G. De Geest, Polymeric multilayer capsules for drug delivery, *Chem Soc Rev* 41(7) (2012) 2867-84.
- [26] P.R. Gil, L.L. del Mercato, P. del_Pino, A. Muñoz_Javier, W.J. Parak, Nanoparticle-modified polyelectrolyte capsules, *Nano Today* 3(3-4) (2008) 12-21.

- [27] A.P.R. Johnston, C. Cortez, A.S. Angelatos, F. Caruso, Layer-by-layer engineered capsules and their applications, *Current Opinion in Colloid & Interface Science* 11(4) (2006) 203-209.
- [28] Y. Yan, G.K. Such, A.P. Johnston, H. Lomas, F. Caruso, Toward therapeutic delivery with layer-by-layer engineered particles, *ACS Nano* 5(6) (2011) 4252-7.
- [29] G. Decher, Fuzzy Nanoassemblies: Toward Layered Polymeric Multicomposites, *Science (New York, N.Y.)* 277(5330) (1997) 1232-1237.
- [30] J.J. Richardson, H. Ejima, S.L. Lorcher, K. Liang, P. Senn, J. Cui, F. Caruso, Preparation of nano- and microcapsules by electrophoretic polymer assembly, *Angew Chem Int Ed Engl* 52(25) (2013) 6455-8.
- [31] S. Sivakumar, V. Bansal, C. Cortez, S.-F. Chong, A.N. Zelikin, F. Caruso, Degradable, Surfactant-Free, Monodisperse Polymer-Encapsulated Emulsions as Anticancer Drug Carriers, *Advanced Materials* 21(18) (2009) 1820-1824.
- [32] J. Cui, Y. Wang, A. Postma, J. Hao, L. Hosta-Rigau, F. Caruso, Monodisperse Polymer Capsules: Tailoring Size, Shell Thickness, and Hydrophobic Cargo Loading via Emulsion Templating, *Advanced Functional Materials* 20(10) (2010) 1625-1631.
- [33] C. Lovelyn, A.A. Attama, Current state of nanoemulsions in drug delivery, *Journal of Biomaterials and Nanobiotechnology* 2(05) (2011) 626.
- [34] K. Pan, Q. Zhong, S.J. Baek, Enhanced dispersibility and bioactivity of curcumin by encapsulation in casein nanocapsules, *Journal of agricultural and food chemistry* 61(25) (2013) 6036-6043.
- [35] A. Gianella, P.A. Jarzyna, V. Mani, S. Ramachandran, C. Calcagno, J. Tang, B. Kann, W.J. Dijk, V.L. Thijssen, A.W. Griffioen, G. Storm, Z.A. Fayad, W.J. Mulder, Multifunctional nanoemulsion platform for imaging guided therapy evaluated in experimental cancer, *ACS Nano* 5(6) (2011) 4422-33.
- [36] T.G. Shutava, P.P. Pattekari, K.A. Arapov, V.P. Torchilin, Y.M. Lvov, Architectural layer-by-layer assembly of drug nanocapsules with PEGylated polyelectrolytes, *Soft Matter* 8(36) (2012) 9418-9427.
- [37] R. Vecchione, G. Iaccarino, P. Bianchini, R. Marotta, F. D'Autilia, V. Quagliarello, A. Diaspro, P.A. Netti, Ultrastable Liquid-Liquid Interface as Viable Route for Controlled Deposition of Biodegradable Polymer Nanocapsules, *Small (Weinheim an der Bergstrasse, Germany)* 12(22) (2016) 3005-13.
- [38] R. Vecchione, U. Ciotola, A. Sagliano, P. Bianchini, A. Diaspro, P.A. Netti, Tunable stability of monodisperse secondary O/W nano-emulsions, *Nanoscale* 6(15) (2014) 9300-7.
- [39] M. Dash, F. Chiellini, R. Ottenbrite, E. Chiellini, Chitosan—A versatile semi-synthetic polymer in biomedical applications, *Progress in polymer science* 36(8) (2011) 981-1014.
- [40] J. Ravindran, S. Prasad, B.B. Aggarwal, Curcumin and cancer cells: how many ways can curry kill tumor cells selectively?, *The AAPS journal* 11(3) (2009) 495-510.

[41] C.A. Schneider, W.S. Rasband, K.W. Eliceiri, NIH Image to ImageJ: 25 years of image analysis, *Nat Methods* 9(7) (2012) 671-5.

Chapter 3

Stimuli-responsive oil-core nanocapsules

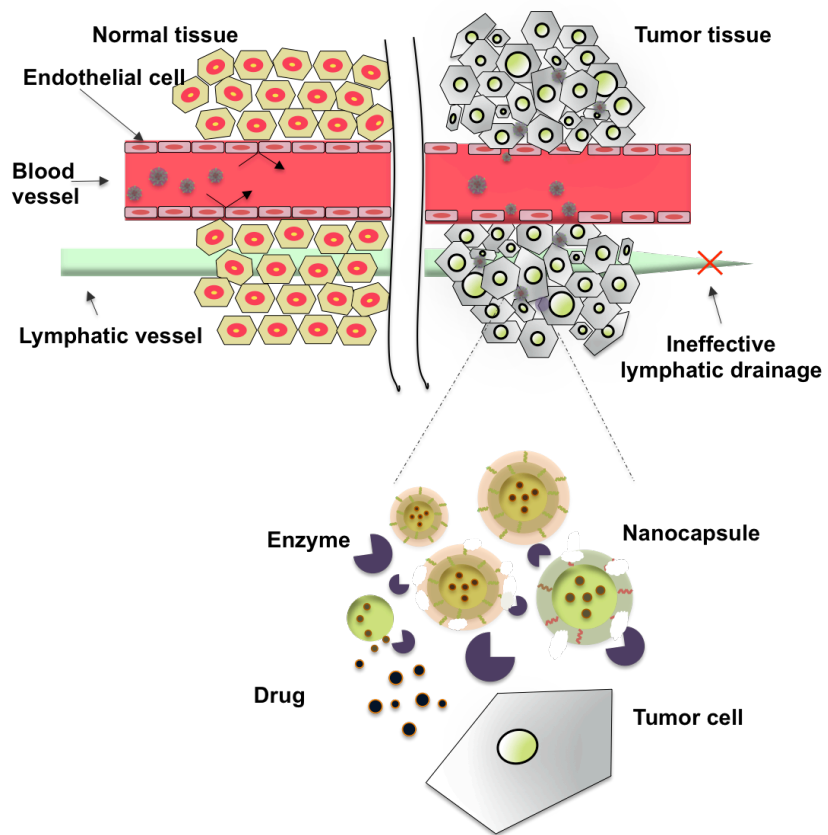


Figure 3.1 A schematic representation of *stimuli*-responsive nanocapsules releasing their payloads upon enzymatic degradation after extravasation in tumor tissue by EPR effect.

Abstract

In the war against cancer nanotechnology-based systems such as nanocapsules play a significant role by enhancing the efficacy of conventional therapies. Here we try to address some major limitations plaguing anticancer drugs, namely poor water-solubility and off-target toxicity. The delivery systems we propose are cross-linked polyelectrolytes nanocapsules based on an oil-core and a matrix metalloproteinase-2 (MMP-2)-sensitive shell. They can load hydrophobic drugs and prevent their systemic leakage. Moreover, thanks to a stability enhancement strategy the system maintained its integrity in physiological conditions up to one month. On the other hand, some preliminary results suggest that the nanocapsules should release their payloads only when they reach the tumor microenvironment, which typically up-regulates MMP-2 expression. These enzymes catalyze the disassembly of the nanocapsules, which are stabilized by an MMP-2-cleavable peptide sequence as cross-linker. This way the drug release should occur in a spatially controlled fashion upon an endogenous *stimulus* coming from the very nature of the tumor itself.

3.1 Introduction

Although pretty much insight has been gained into tumor biology and giant leaps have been made in diagnostic devices, cancer still remains one of the most devastating diseases in the world and its treatment an open challenge. Current anticancer strategies are based on surgery, radiation and chemotherapeutic drugs, which often also kill healthy cells causing severe toxicity to the patient. Therefore, a new type of weapon in the war on cancer is needed. Typically, conventional chemotherapeutic approaches make use of poor water-soluble agents, which allow for very little control in terms of where they are distributed in the body and how fast they are cleared. This in turn implies a poor biodistribution and pharmacokinetics of the drug, which dramatically decrease its therapeutic index while increasing off-target toxicity.

It is in this scenario that the concept of enhanced control and specificity has emerged as one of the main themes in nanomedicine [1] and a new generation of nanocarriers for the controlled and selective release of anticancer drugs has blossomed. The technological leap that especially the past decade has witnessed deals with on-demand drug delivery allowing for spatiotemporal and dosage control therapeutic profiles in response to specific *stimuli* [2]. These nanocarriers may be engineered to be sensitive to either exogenous or endogenous *stimuli*. For example, among the extracorporeal physical *stimuli* that can be applied, one can think to use light at a specific wavelength to trigger on-demand release from photosensitive systems [3]. The remote control of drug release can also be achieved by thermo- [4], magnetic- [5] or ultrasound-sensitive nanoparticulate systems [6].

On the other hand, it is also smart taking advantage of specific microenvironmental changes associated with neoplastic diseases to stimulate spontaneously tailored release profiles. The most explored options among potential endogenous *stimuli* associated to tumor microenvironment include the

lowered interstitial pH [7], the altered redox potential due to higher glutathione concentration [8] and the up-regulation of certain enzymes such as matrix metalloproteinases (MMP) [9]. In particular, this proteolytic family of enzymes appears to play a central role in tumor angiogenesis, progression and invasion by remodeling of extracellular matrix (ECM) [10]. Therefore, the use of MMP cleavable peptides in conjugation with nanoparticle delivery systems holds great promise for the development of new therapeutic formulations. For example, MMP-2 enzymes (also known as gelatinase A; Mw: 72 kDa) hydrolyze type IV collagen, which is a major constituent of tumor ECM [11]. There are several examples in literature where MMP-2 are used as a trigger to promote selective drug release to tumors from nanocarriers engineered with peptide sequences sensitive to the catalytic activity of these enzymes [12] [9, 13].

On the other hand, to improve the pharmacokinetics of the drug and reduce its side effects, it is also crucial to prevent systemic leakage of the payload from delivery systems. To this aim enhancing the stability of nanocarriers during blood circulation can really make the difference in the accumulation of the drug at the tumor site [14] [15].

Based on all these considerations, here we propose a strategy that attempts to face at one time two major issues related to the delivery of chemotherapeutic agents: the stability of the nanocarrier in the blood and the selective release of the drug to the target tissue. Following this aim, the main goal of this work is to provide NCs with two complementary features. On the one hand, we want to enhance NC stability in media where they could potentially undergo disassembly and thus lead to an uncontrolled release of the payload. On the other hand, we want to trigger the destabilization of the NCs once they explore a specific tumor microenvironment in order to promote the drug release. Thus, the delivery systems we propose are cross-linked polyelectrolytes NCs based on an oil-core and an MMP-2-responsive shell. In particular, their core/shell architecture is designed to encapsulate relatively large amounts of drug. The lipid core is based

on a monodisperse 20% v/v O/W NE, preloading Paclitaxel as a chemotherapeutic lipophilic agent. The polyelectrolyte shell adds potential to the bare liquid reservoir since it protects the payload from the outside, provides a hydrophilic interface and allows for a tunable release. The polymers we employ are nature-derived polysaccharides, namely chitosan and heparin which are assembled around the lipid core by a facile Layer-by-Layer (LbL) method [16]. This technique has emerged as one of the most versatile and controlled method to deposit ultrathin polymer layers around virtually any sort of templates, mainly driven by electrostatic forces among polyelectrolytes of opposite charge. True is that despite the several advantages offered by LbL, the only electrostatic interactions might turn out too weak for the stability of the NCs in physiological environment. Thereby, to prevent premature disassembly of the NCs and consequent systemic leakage issues, we provide a covalent stabilization by chemically cross-linking the polyelectrolytes pairs of NCs shell *via* click chemistry [14]. The chemical reaction we chose for this purpose is the thiol-ene click reaction, a metal catalyst-free approach to form a tioether bond between thiols and alkenes. Besides being highly biocompatible, this chemical reaction is performed under mild conditions and allows for elegant design of supramolecular structures [17] [18]. In this context, we use an MMP-2 sensitive peptide (Gly-Pro-Leu-Gly-Ile-Ala-Gly-Gln) [13] [19, 20] as chemical linker between the polymer layers of the shell. We have slightly modified this sequence in order to tag it with a fluorophore and allow for coupling reaction with heparin, on one side, and click reaction with cysteine-modified glycol chitosan, on the other side. Then, we assemble the pre-functionalized polysaccharides onto the NE template by LbL deposition and cross-link them through the peptide linker under UV light. This way we obtain NCs loading a powerful chemotherapeutic agent, which in principle are physically stable until they explore the higher concentration of MMP-2 within tumor microenvironment. The catalytic activity of the enzymes, indeed, induces the cleavage of the peptide

linker that has provided the enhanced stability to the NCs until then. The NCs undergo an MMP-2 mediated disassembly which promotes the release of the drug preferentially at the tumor site.

In the light of these considerations, here we try to address the off-site toxicity big issue combining a stability enhancement and a *stimuli*-responsive drug release approach. The first prevents systemic leakage and off-target release through the cross-linking of the NC shell. The latter allows for a spatially controlled release of the drug through the cleavage of the MMP-2 sensitive shell preferentially in tumor microenvironment. This way drug release occurs upon an endogenous *stimulus* that comes from the very nature of the tumor itself.

3.2 Results and Discussion

Solid phase peptide synthesis

In order to achieve a stabilization/destabilization mechanism for our NCs, we carefully designed a double-feature peptide linker to embed within the polymer layers of NC shell. In the first place, we identified an amino acidic sequence (Gly-Pro-Leu-Gly-Ile-Ala-Gly-Gln) that was sensitive to MMP-2 catalytic activity. Then, we modified it by adding an allylated aspartic acid to perform thiol-ene click reaction with thiolated chitosan. We also introduced in the sequence an Mtt-lysine which provided the functional moiety to attach rhodamine B to the peptide side chain. Therefore, the resulting modified sequence is Lys-Gly-Pro-Leu-Gly-Ile-Ala-Gly-Gln-βAla-Asp(allyl) (see **Figure 3.2.1** for a schematic representation).

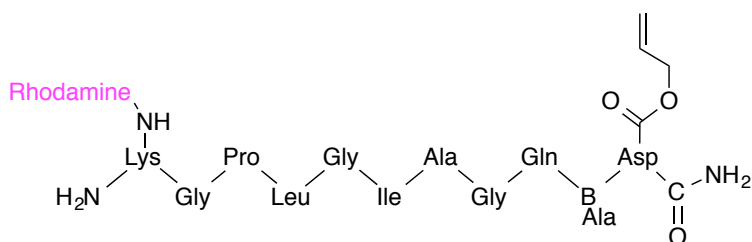


Figure 3.2.1 MMP-2 peptide sequence modified with rhodamine and allylated aspartic acid.

At the same time, we applied the same strategy for the preparation of a control sequence named RHOD-ctrlPEP (Lys-Leu-Gln-Gly-Ile-Gly-Pro-Gly-βAla-Asp(allyl)), which differs from RHOD-PEP only for the disposition of the amino acids of active domain. We monitored the peptide during all the steps of its modification by mass spectrometry. In **Figure 3.2.2** we report the mass spectra of the peptide after synthesis, coupling with rhodamine B and Fmoc

deprotection. First we confirmed the purity and quality of the peptide (Fmoc-PEP) that we synthesized by a solid phase approach. In **Figure 3.2.2a** we report the molecular peak corresponding to the theoretic molecular weight of Fmoc-PEP. Then, after removing the orthogonal Mtt protecting group from lysine in mild acidic conditions, we labeled the peptide with rhodamine B. The effective conjugation is confirmed by the second and third charge mass peak of FMOC-RHOD-PEP (**Figure 3.2.2a**). Finally, we checked for complete Fmoc deprotection of the rhodamine labeled peptide (RHOD-PEP) before performing the coupling reaction with heparin. In **Figure 3.2.2c** RHOD-PEP exact mass and first and second charge are reported. Equivalent results were obtained also for the control peptide sequence (ctrlPEP).

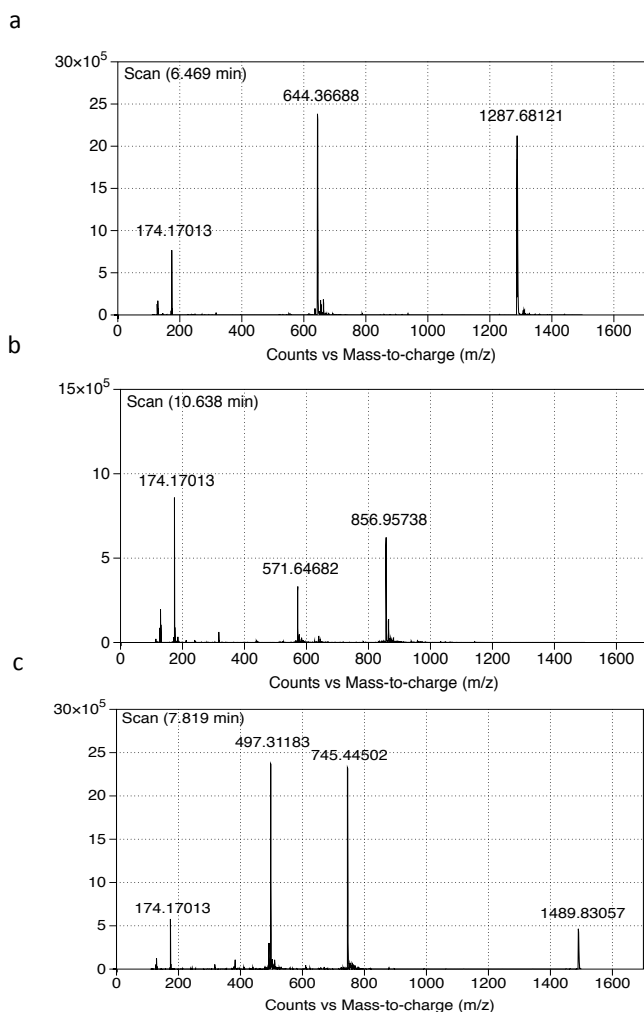


Figure 3.2.2 Mass spectra of Fmoc-protected peptide after synthesis (a), Fmoc-protected peptide after coupling with rhodamine B (b), rhodamine labeled peptide after Fmoc deprotection (c). Please note that the intensity value of 174.17013 recurring in all three spectra corresponds to the internal standard.

Heparin – rhodamine peptide conjugation

In order to embed the MMP-2 sensitive linker within the polymer layers of the NCs we conjugated the modified peptide sequence with heparin. By condensation reaction between peptide N-terminus and heparin carboxylic acids moieties we achieved around 50 % substitution of the polymer chains. We

estimated such value by fluorimetric assay measuring rhodamine signal of the heparin-peptide conjugate ($\lambda_{\text{ex}}/\lambda_{\text{em}} = 550/570 \text{ nm}$). We, indeed, correlated this fluorescence intensity to a rhodamine-peptide calibration curve acquired within a range of concentrations comprised between 0 and 0.065 mM (**Figure 3.2.3**).

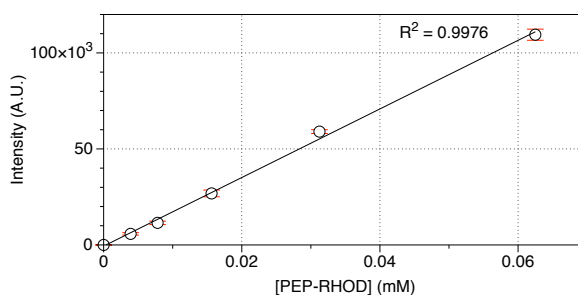


Figure 3.2.3 Calibration curve to calculate the substitution degree of heparin with PEP-RHOD. The curve was recorded by a spectrofluorimeter measuring the fluorescence intensities from solutions at different concentrations of PEP-RHOD.

In **Figure 3.2.4** we provide a schematic representation of the heparin peptide conjugate that for the sake of shortness we named HEP-RHOD-PEP.

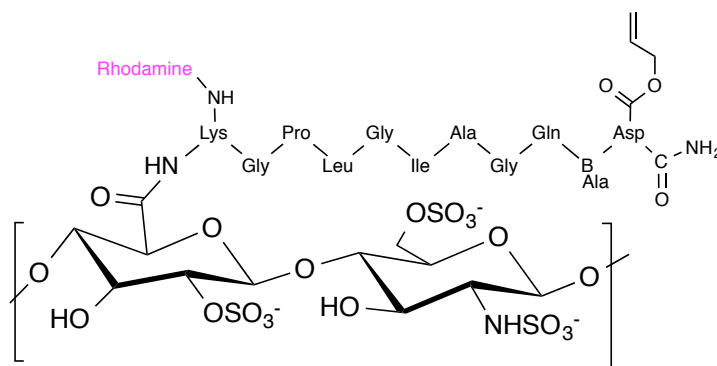


Figure 3.2.4 Heparin functionalized with the fluorescent MMP-2 peptide.

Glycolated chitosan thiolation with N-acetyl-L-cysteine

Glycolated chitosan was partially substituted at the free amine groups with N-acetyl-L-cysteine (NAC) in order to provide the chains with thiol moieties. A typical amidation reaction was carried in presence of water soluble coupling agents, namely carbodiimide (EDC, ethyl-3-(3-dimethylaminoisopropyl)-carbodiimide) and 1-hydroxy-1,2,3-benzotriazole (HOBt) (in **Figure 3.2.5** a schematic representation of the chemical reaction is provided). Although this chemistry is widely used, it is rarely applied to polysaccharides especially in the case of chitosan, since it is difficult to substitute amine groups because of the poor solubility and reactivity of the polymer. The solubility issue was addressed using the glycolated chitosan in place of the LMW chitosan. In fact, the ethylene glycol moieties allowed for water solubility of the polymer even at neutral pH. On the contrary, LMW chitosan requires an acidic pH to reach complete dissolution through amines protonation. This constraint strongly limits the effectiveness of the coupling reaction, which in contrast requires a slightly basic pH in order to make the amines nucleophile. The degree of thiolation that was reached based on our scheme of reaction was assessed by Ellman's test. This colorimetric assay, indeed, may highlight the concentration of free thiols by reaction with DTNB (also known as Ellman's reagent), which absorbs at 412 nm.

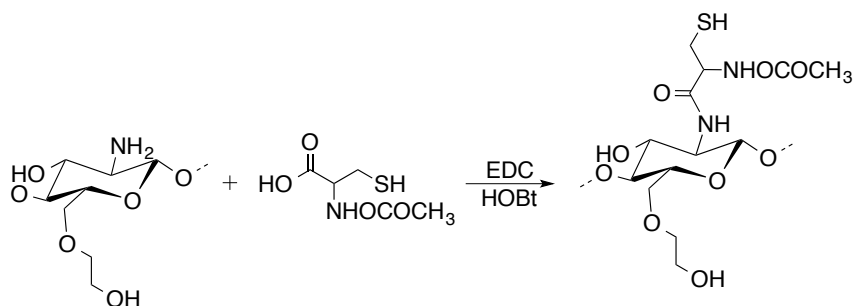


Figure 3.2.5 Thiolation of glycol chitosan with NAC by EDC/HOBt chemistry.

The first step in the construction of the crosslinked polymer NCs was preparing an O/W NE pre-loading Paclitaxel. Following an optimized procedure (see chapter 2) we obtained narrowly distributed NEs, as shown by the DLS and the cryo-TEM reported in **Figure 3.2.6a** and b, respectively. The Paclitaxel (PXL) concentration in the overall volume of the NE was 37,5 $\mu\text{g}/\text{ml}$ (44 μM).

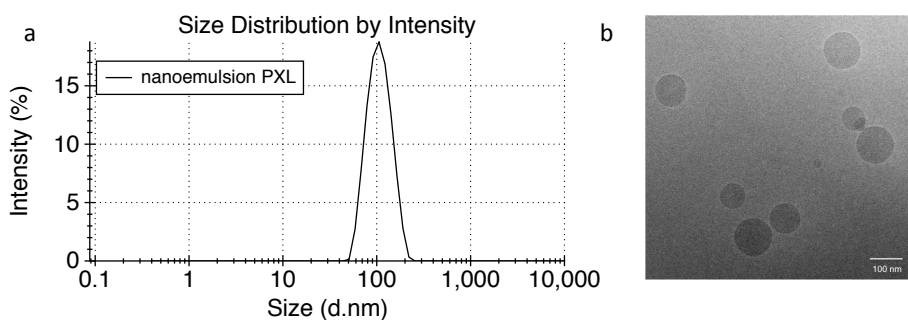


Figure 3.2.6 Average size of PXL loaded NE by DLS (a) and by cryo-TEM (b). (Scale bar: 100 μm).

Starting from these oily templates we built our NCs assembling the modified polymers through a customized LbL procedure (see chapter 2 for more details on the method). First, we deposited a thiolated glycol chitosan (GC-NAC) layer on the negatively charged NEs. The GC-NAC monolayer NCs was then coated with a second layer of functionalized heparin. Finally, a last layer of GC-NAC was deposited. This way we obtained oil-core narrowly distributed trilayer NCs coated with naturally derived polyelectrolytes embedding an MMP-2 sensitive substrate. We shortly named this trilayer as MMP NCs. We also prepared two control series of trilayers based on non-functionalized heparin (HEP) and heparin modified with the control sequence peptide (HEP-ctrlPEP), which in the following will be recall as NF NCs and ctrlMMP NCs, respectively. The average size and the Z-potential of the three types of trilayer NCs at each step of the deposition process are summarized in **Figure 3.2.7**. It is noteworthy, that

these results were achieved following an optimized LbL deposition procedure (see chapter 2 for more details), which preserved the small size and narrow size distribution (PDI \approx 0.1) of the starting NE. In fact, dealing with naturally derived polymers modified with sterically bulky pendant molecules, may really plague the deposition process. We also proved that the rhodamine labeled peptide was effectively embedded within the NC shell by confocal microscopy, as shown in **Figure 3.2.8**.

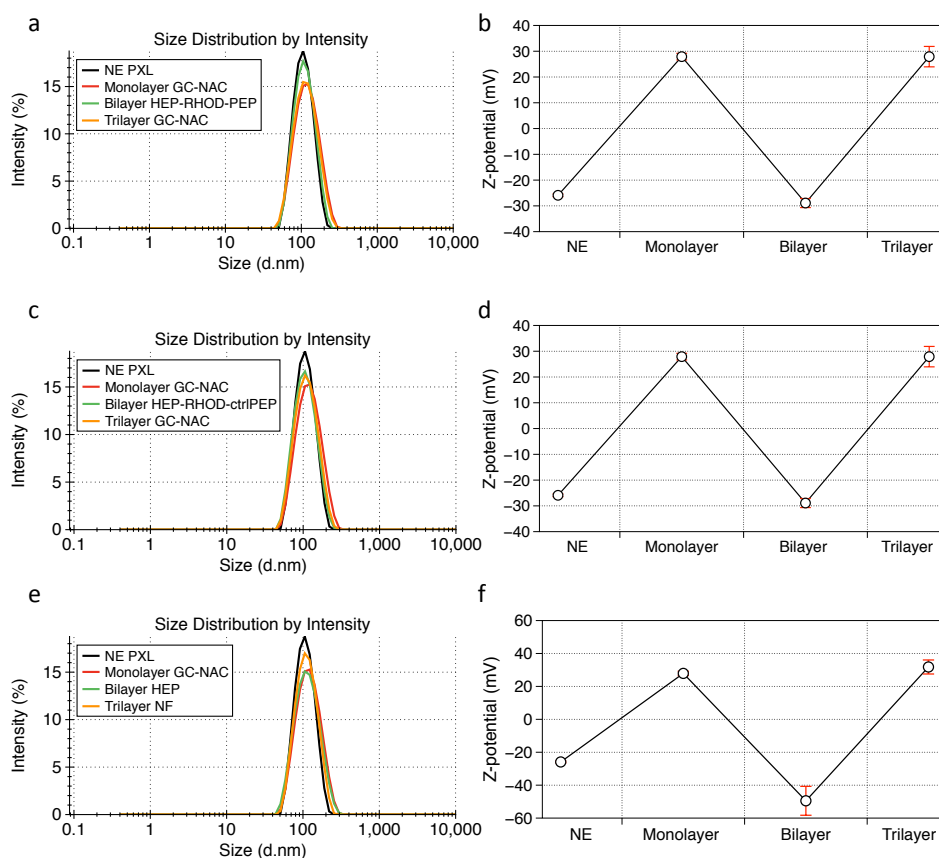


Figure 3.2.7 Size distribution and Z-potential of the three types of trilayer NCs: MMP NCs (a,b); ctrlMMP NCs (c,d); NF NCs (e,f).

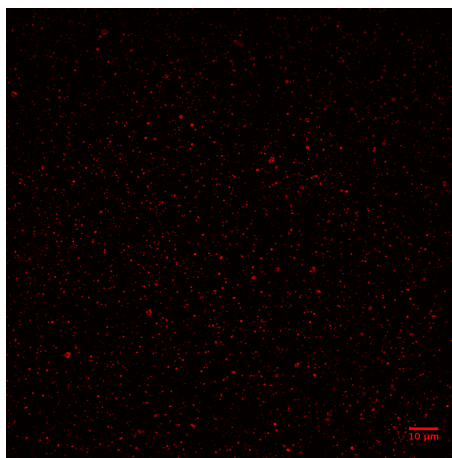


Figure 3.2.8 Confocal fluorescence microscope image of NCs bilayer coated with rhodamine-peptide modified heparin. (Scale bar:10 μm).

Stability enhancement of MMP-2 trilayer nanocapsules

We then exposed part of the as prepared trilayer NCs to UV light ($\lambda = 254$ nm) in order to promote the formation of a tioether bond between the thiol moieties on GC-NAC and the alkene groups on the side chain of the peptide. The click reaction effectively brought to an enhancement of the trilayer stability through the crosslinking of the polymer layers. We performed the stability test by monitoring the size and the PDI of crosslinked and not-crosslinked trilayers in media with different pH and ionic strength, namely acid water (pH 4) and phosphate buffer (PBS 10 mM; pH 7.4). As highlighted by the size and PDI measurements reported in **Figure 3.2.9a** and **b** respectively, when dispersed in PBS, the crosslinked NCs show an initial swelling (≈ 100 nm), while the PDI does not seem affected by the change of medium. Moreover, this condition keeps constant over about one month. On the other hand the not-crosslinked

trilayers completely lose their dimensional characteristics after only one week increasing both their size and PDI in an uncontrolled fashion. Our explanation to this behaviour is that the change of medium causes an expected weakening of the electrostatic interactions between the layers of the NC shell. Due to the lower attraction, the oppositely charged layers get more distant from each other, thus leading to a larger NC size. However, only in the case of crosslinked NCs, the polymer layers are still hold together by some chemical linkages provided by the peptide linkers. These covalent constraints prevent the NC size to further increase, while keeping it to a constant value. This, in turn, would also justify a constant value of the PDI over time since the size increase is uniformly distributed among all the crosslinked NCs.

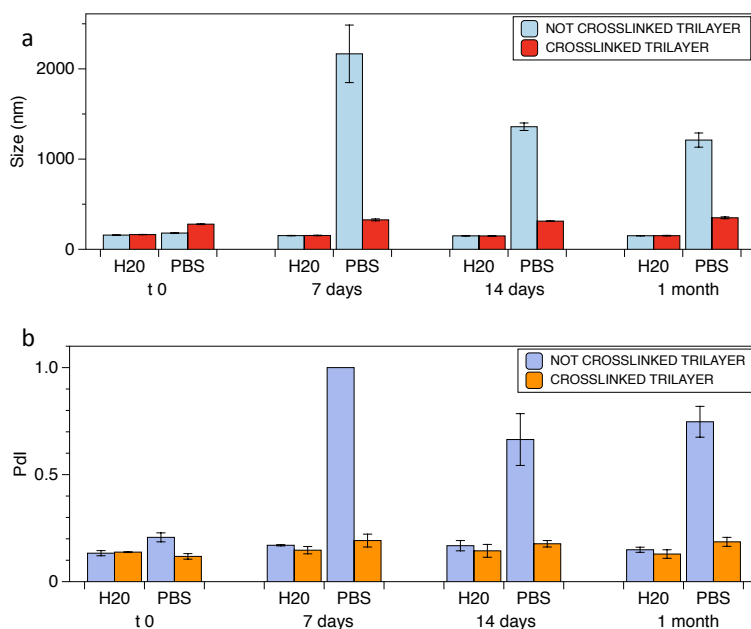


Figure 3.2.9 Size (a) and PDI (b) changes over time both in acid water and PBS of crosslinked and not crosslinked (HEP-PEP) NCs by DLS.

Cytotoxicity and Confocal Microscopy Imaging of MMP-2 Sensitive nanocapsules

To evaluate the cytotoxic effect of MMP-2 sensitive NCs and NF NCs when exposed to MMP-2 enzyme, preliminary tests were performed *in vitro* by means of Alamar Blue assay on HDF and U87 cells, which are healthy and tumor cell lines, respectively. The latter were chosen since they were already characterized in terms of MMP-2 expression levels and activity in a previous work of our group [19]. **Figure 3.2.10** shows cell viability percentage of treated cells normalized to non-treated cells. MMP-2 sensitive NCs, pre-treated for 24 h with MMP-2 activated enzyme, showed a cytotoxic effect in all the cell types. On the other hand, a lower cytotoxic effect was observed for the MMP-2 sensitive NCs not pretreated with the enzyme. In particular, HDF and U87 cells after 24 h of exposure to MMP-2 sensitive NCs pre-treated with the enzyme showed respectively a 30% and 20% decrease in cell viability when compared to the control group. This gap is maintained constant increasing the incubation time. These data displayed a better performance of the enzyme pre-treated NCs, in which the shell is destabilized because of the peptide sequence that facilitates drug release from the core cleavage. This happens because, as already mentioned, the peptide sequence both stabilizes the NCs and provides the *stimuli*-responsive properties. Furthermore, these data are in accordance with the spectrofluorimetric analysis performed on the PS model NCs which show a RHOD content in the supernatant 5.3 fold higher for the treated NCs when compared to the untreated ones. Finally, control experiments were carried out treating cells with the non-functionalized NCs both in presence and absence of enzyme pre-treatment. Collectively we may observe a more relevant cytotoxic effect of the non-functionalized NCs compared to the MMP-2 responsive ones; this is probably due to the absence of the stabilizing element, namely the peptide. However, these preliminary results have to be supported by further experiments. To verify shell degradation after the exposure to the enzyme,

model PS core NCs were used for imaging analysis by confocal microscopy. These model NCs were chosen for this experiment since their solid core allows for a separation of the degraded shell from the core through centrifugation (see Material and Methods section).

In particular, HDF and U87 cells were observed by confocal microscopy after 24 h of incubation with PS nanoparticles as negative control, enzyme treated and enzyme untreated PS core MMP-2 sensitive NCs and enzyme treated and enzyme untreated PS core ctrlMMP NCs.

Figure 3.2.11 and **3.2.12** show NCs distribution in HDF and U87 cells respectively.

Figure 3.2.11b and **3.2.12b** shows the presence of a diffused cytoplasmic green fluorescent signal due to nanoparticle uptake by the cells.

Figure 3.2.11c, **3.2.12c** and **3.2.11d**, **3.2.12d** show cells treated with MMP-2 sensitive NCs with and without the enzyme treatment, respectively. In particular, in panel c only a spotted green fluorescent signal is visible, while panel d displays a yellow spotted fluorescent signal due to the co-localization between the green signal of the PS core and the red signal of the RHOD-peptide that composes the NC shell.

Finally, **Figure 3.2.11e**, **3.2.12e** and **3.2.11f**, **3.2.12f** show cells treated with ctrlMMP NCs with and without the enzyme treatment, respectively. All the panels show a yellow spotted fluorescent signal derived from the co-localization of the green signal of the PS core with the red signal of the RHOD-peptide that composes the NC shell.

Since co-localization occurred in both cases, we may assume that the enzyme pre-treatment did not cause the disassembly of the NC shell. This happens because the ctrl peptide is not specific for MMP-2 enzyme cleavage.

Taken together these preliminary results clearly show that the enzyme pre-treatment of the MMP-2 sensitive NCs causes a disassembly of the shell that does not occur without the enzyme treatment. Moreover, the enzymatic

disassembly of the shell only occurs if the NCs are functionalized with an MMP-2 sensitive peptide sequence.

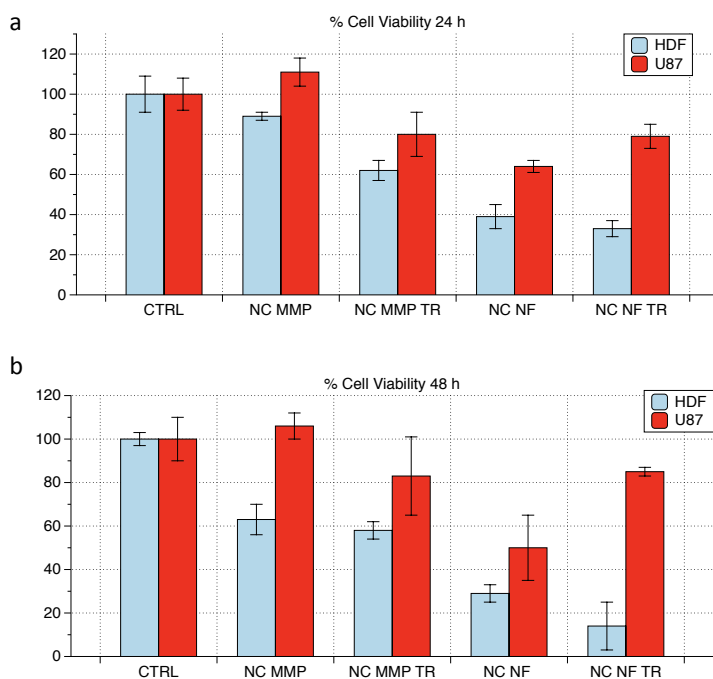


Figure 3.2.10 Cytotoxicity assay of MMP-2 sensitive NCs, the figure shows cell viability of MMP-2 sensitive NCs pre-treated, non-functionalized NCs and non-functionalized NCs pre-treated in HDF and U87 cells after (a) 24 and (b) 48 h of incubation. Cell viability was expressed as percentage compared to control cells.

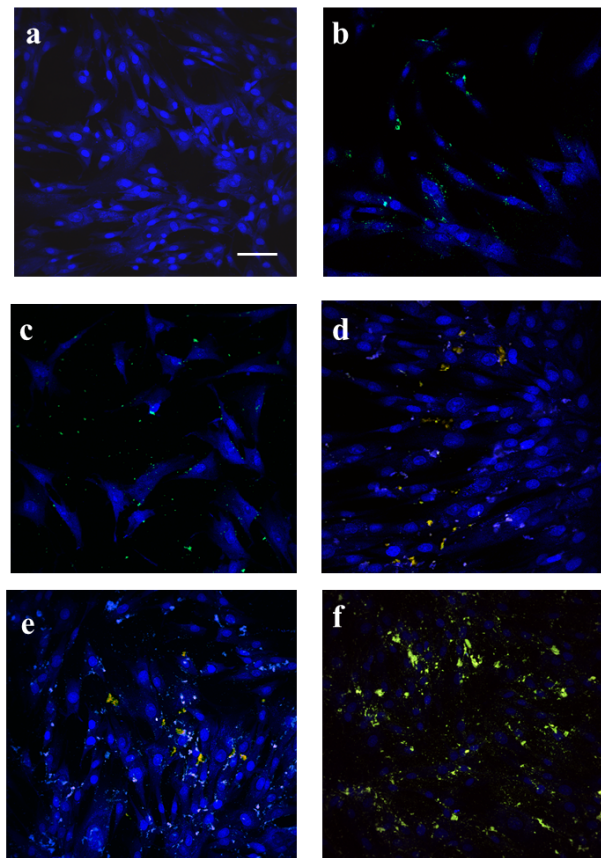


Figure 3.2.11 Confocal images of HDF cells. HDF cells (a), cells treated with PS (b), MMP-2 sensitive pre-treated NCs (c), MMP-2 sensitive NCs (d), ctrlMMP NCs non-treated (e) and ctrlMMP NCs (f) after 24 h of NCs exposure. PS nanoparticles are in green, RHOD-peptide is in red and cell nuclei and cytoplasm is in blue. Colocalization of RHOD-peptide and PS nanoparticles may be seen in yellow. (Scale bar: 75 μ m).

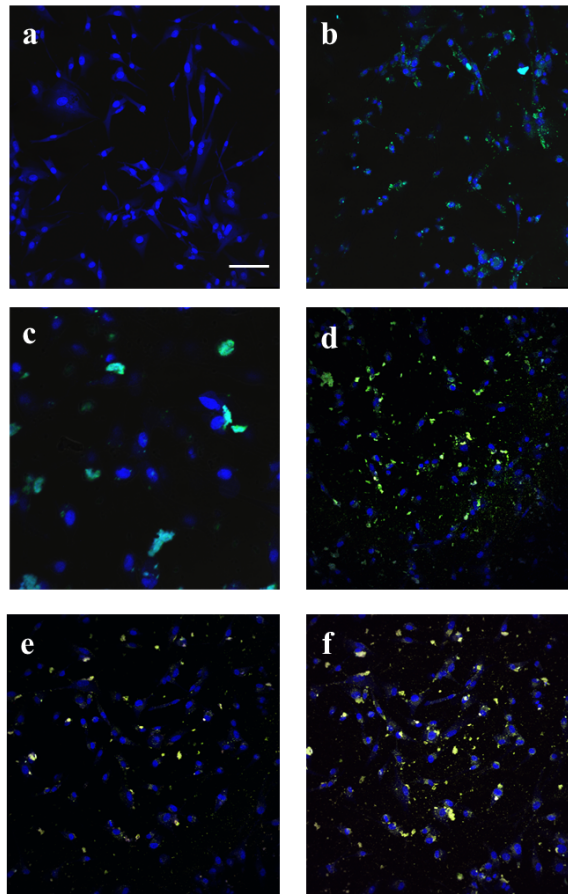


Figure 3.2.12 Confocal images of U87 cells. U87 cells (a), cells treated with PS (b), MMP-2 sensitive pre-treated NCs (c), MMP-2 sensitive NCs (d), ctrlMMP NCs pre-treated (e) ctrlMMP NCs (f) after 24 h of NC exposure. PS nanoparticles are in green, RHOD-peptide is in red and cell nuclei and cytoplasm is in blue. Colocalization of RHOD-peptide and PS nanoparticles may be seen in yellow. (Scale bar :75 μm).

3.3 Conclusions

In this work we focused on one of the major concern related to the administration of anticancer drugs, namely off-target toxicity. Although nanomedicine struggles to find always-new nanotechnology based solutions, there is still a tremendous need for drug delivery systems capable to maximize the therapeutic index and to drastically reduce side effects.

To this aim we designed and prepared stabilized oil-core polymer NCs allowing for a spatially controlled release of their payload in response to an endogenous *stimulus* coming from the very nature of the tumor.

Thus we pre-loaded a finely dispersed O/W NE with a relatively large amount of a common chemotherapeutic agent. Then we coated the NE with nature-derived polymers that we had previously modified to allow for their chemical crosslinking based on a catalyst free click chemistry approach.

This way we obtained narrowly distributed polymer NCs showing enhanced stability in physiological media over 1 month compared to their basic LbL counterparts.

Furthermore, the NCs demonstrated to be responsive to the catalytic activity of MMP-2, undergoing a disassembly of their polymer shell after exposure to the enzymatic environment. Indeed, to achieve a tumor site-specific drug release mechanism we used an MMP-2 sensitive peptide as cross-linker between the polymer layers. Therefore, the NCs keep their stability until they reach the tumor microenvironment where MMP-2 are usually up-regulated so that it is the tumor itself that triggers the release of the drug.

In conclusion, this strategy may be a viable route to address with a single elegant solution both the NCs stability issue and the spatially controlled release requirement, thus contributing to increase the efficacy of the current anticancer therapies.

3.4 Future Perspectives

The results of the biological assays stem from an early step in understanding NCs behavior in physiological-like conditions. In particular, a more complex *in vitro* cancer model may be used to test the NCs performance. In this context tumor spheroids are, for example, a relevant *in vitro* model able to better mimic the 3D tissue architecture if compared to standard 2D models [19]. In this case, it would be possible to test NCs cytotoxicity as a function of endogenous MMP-2. In particular, the use of two diverse cell lines expressing different levels of endogenous MMP-2 may help to better understand NCs ability to trigger a specific release in response to an endogenous *stimulus* usually overexpressed in tumor tissues.

3.5 Materials and Methods

Materials

Chitosan low molecular weight (CT-LMW, 90-150 kDa), heparin sodium salt (from porcine intestinal mucosa), 1-hydroxybenzotriazole hydrate (HOBt), acetic acid, sodium acetate, sodium chloride, N-acetyl-L-cysteine (NAC), allylamine, sodium nitrite, methanol, ammonium hydroxide solution, sodium borohydride, hydrochloric acid, sodium hydroxide, deuterium oxide (D₂O), dithiobis(2-nitrobenzoic acid) (DTNB), fluorescein isothiocyanate (FITC), N-(3-Dimethylaminopropyl)-N'-ethylcarbodiimide hydrochloride (EDC), O-benzotriazole-N,N,N,N'-tetramethyluroniumhexafluorophosphate (HBTU), N,N-diisopropylethylamine (DIPEA), anhydrous N,N-dimethylformamide (DMF), piperidine, trifluoroacetic acid (TFA), Triisopropylsilane (TIS), dichloromethane (DCM), 2-(N-Morpholino) ethanesulfonic acid (MES) sodium salt, HEPES, p-aminophenylmercuric acetate (APMA), acetonitrile (ACN) HPLC grade water, 1-[bis(dimethylamino)methylene]-1H-1,2,3-triazolo[4,5-b]pyridinium 3-oxid hexafluorophosphate (HATU reagent) and buffer solutions were obtained from Sigma–Aldrich (Saint Louis, MO). Recombinant Human Matrix metalloproteinase-2 (MMP-2) was purchased from Peprotech Inc. (Rocky Hill, NJ). Soy-bean oil (density at 20 °C of 0.922 g/ml) and Lipoid E80 lecithin (egg lecithin powder 80 85% enriched with phosphatidyl choline and 7-9.5% content in phosphatidyl ethanolamine) were purchased from Lipoid. Glycol chitosan (GC) was purchased from Wako Chemicals. Carboxyl latex beads (4% (w/v), 0.1 μm) and FluoSpheres[®] (Carboxylate-Modified Microspheres, 0.1 μm, yellow-green fluorescent (505/515), 2% solids) were purchased from Invitrogen. Dialysis membranes were purchased from Spectrum Laboratories Inc.

Peptide synthesis

MMP-2 sensitive peptide (NH₂-Lys-Gly-Pro-Leu-Gly-Ile-Ala-Gly-Gln-βAla-Asp(allyl)-COOH) was synthesized in a modified version, with a 4-Methyltrityl (Mtt) protected lysine at the N-terminal, and a beta alanine spacer and an allylated aspartic acid at the C-terminal. It was employed the solid-phase method and standard Fmoc strategies. Rink-amide resin (substitution 0.7 mmol/g) was used as solid support. Activation of amino acids was achieved using 2-(1H-Benzotriazole-1-yl)-1,1,3,3-tetramethyluroniumhexafluorophosphate: hydroxybenzotriazole: N,N-diisopropylethylamine (HBTU/HOBt/DIEA) (1 : 1 : 2). All couplings were performed for 15 min and deprotections for 10 min. Peptides were not removed from the resin, after acetylation step to allow coupling reaction with rhodamine while still attached. Peptides purity and identity were confirmed by LC-MS (Agilent 6530 Accurate-Mass Q-TOF LC/MS spectrometer). Purified peptide was lyophilized and stored at 4 °C until use.

Reagents for peptide synthesis (Fmoc-protected amino acids, resins, activation, and deprotection reagents) were from Iris Biotech GmbH.

Labeling reaction

Before the coupling reaction of peptides with rhodamine, the Mtt group protecting the side chain of the lysine residue was selectively removed using 1% TFA in DCM plus 1-5% TIS for quenching the trityl cations released. These conditions allowed the peptide to remain attached to the support although Rink amide is an acid-labile resin.

Pre-swelled dry resin (100 mg) was repeatedly rinsed with the as prepared deprotection mixture of solvents 2 minutes and flushed. Complete deprotection of amines was assessed by Kaiser test and mass spectrometry.

For labeling reaction, carboxylated rhodamine and activating agents (EDC/HOBt) (excess 2 with respect to the theoretic mass of peptide) was let reacting overnight with the pre-swelled dry resin in DCM containing DIPEA. At the end of reaction the resin was washed several times with DMF and the last 6 washes were performed alternating DCM and Methanol. In order to check for left free amines in the side chain of the peptide, Kaiser test and LC/MS were performed at the end of reaction. Then, only before coupling reaction with heparin, the peptide was deprotected from Fmoc at the N-terminus and removed from the resin. Experimentally, Fmoc groups were removed with 20% piperidine solution in DMF. After washing, Kaiser test was performed to detect that all the N-terminus amines were free.

Peptides were removed from the resin by treatment with a TFA/TIS/H₂O (95 : 2.5 : 2.5, v/v/v) mixture for 90 min at room temperature, then, crude peptide was precipitated in cold diethyl-ether, dissolved in a water/acetonitrile (1:1, v/v) mixture, freeze-dried for 48h and stored at -20°C.

All the procedures described for both the synthesis and the labeling of the peptide were applied also to the control sequence peptide.

Heparin - peptide coupling reaction

The condensation of the carboxylic acids of heparin chains with the peptide N-terminus was carried in slightly basic conditions using a classic EDC/NHS chemistry.

In a typical procedure, heparin (10 mg, 1 equiv) was dissolved in 1 ml of carbonate buffer (pH 7.8). Then, 3.4 mg (22 equiv) of EDC*HCl were added and the solution was stirred at room temperature for 30 min. Two milligrams (22 equiv) of NHS were then added, and the solution was stirred at room temperature for 3 h. Twenty-one point nine milligrams (1 equiv) of rhodamine-labeled peptide were added, and the mixture was stirred overnight. Then, the

product of reaction was dialyzed using a 6-8 kDa bag against a mixture ACN/water 30:70 for 48 h. The purified conjugate was finally freeze-dried and stored at -20°C.

The substitution degree of heparin was assessed by measuring the fluorescence intensity of the rhodamine-peptide after calibration with a water solution of rhodamine-peptide at different concentrations using a spectrofluorimeter (EnSpire 2300 PerkinElmer).

Oil-in-Water nanoemulsion

The O/W nano-emulsion was prepared as previously described (see chapter 2). Briefly, the oil phase was prepared by adding an exact amount of Lipoid E 80 to the soy-bean oil at 60 °C and then sonicated with an immersion sonicator (Ultrasonic Processor VCX500 Sonic and Materials). To obtain the pre-emulsion, the oil phase was added dropwise to a weighted amount of aqueous phase (Milli-Q water) and mixed using the immersion sonicator. The pre-emulsion was finally passed at 2000 bar through the high-pressure valve homogenizer (Microfluidics M110PS) to obtain the final nano-emulsion.

Modification of glycol chitosan with N-Acetylcysteine

Thiolation was performed on glycol chitosan (GC, chitosan conjugated with ethylene glycol) according to a procedure previously reported [21]. In the typical procedure, 0.5 mmol of the chitosan substrate were dissolved in 10 ml of Milli-Q water. In the first place, the pH was adjusted to a value of 4 with HCl 1 M to allow complete dissolution. Then, amounts of NAC and coupling agents were added to the solution according to the following molar ratio HOBt : GC : NAC

: EDC = 1 : 1 : 4 : 16. Then the pH was raised and maintained to a value of 6.8 throughout the reaction time (6 h). The reaction proceeded at room temperature. The product was then purified by dialysis four times against water containing 1% (w/v) NaCl and acidified with HCl at pH = 3, four times against water acidified at pH = 3. Finally, the purified product was freeze-dried for 48 h.

Total and free thiols were determined using a colorimetric assay, the Ellman's test. In particular, after reaction of thiolated chitosan with a DTNB solution at 25 °C for 2 h, absorbance was registered at 412 nm using a Varian Cary Scan 100 Spectrophotometer.

LbL deposition of functionalized polymers on O/W nanoemulsion

Monolayer, bilayer and trilayer were obtained by a customized LbL deposition procedure already reported in the materials and methods section of chapter 2. Briefly, the trilayer NCs were prepared by aid of two syringe pumps (HARVARD APPARATUS 11 PLUS) and an ultrasonic bath (FALC INSTRUMENTS) under specific flow and ultrasounds conditions. Starting from the negatively charged NEs a GC-NAC layer was first deposited. Then, a negatively charged second layer was deposited by mixing the monolayer suspension with a HEP-RHOD-PEP aqueous solution. Finally, the bilayer was mixed with a solution of GC-NAC to give the MMP-2 responsive trilayer with the following final concentrations: 0.25% wt% oil - 0.025 wt% GC-NAC - 0.0069 wt% HEP-RHOD-PEP - 0.02 wt% GC-NAC. The same procedure for the preparation of trilayer NCs was followed also using the control peptide modified heparin (HEP-RHOD-ctrlPEP) and the non functionalized heparin

(HEP) the trilayers were prepared following but with the same final trilayer concentrations as for the one prepared with HEP-RHOD-PEP.

LbL deposition of functionalized polymers on polystyrene carboxylated nanoparticles

The same procedure described in the previous paragraph was employed for the assembly of all the three kinds of trilayers also around polystyrene nanoparticles (PS NPs) for imaging purposes. In this case the final concentrations for all the three kinds were: 0.04% wt% PS NPs - 0.032 wt% GC-NAC - 0.0064 wt% HEP-RHOD-PEP - 0.032 wt% GC-NAC.

Photoreaction of the multilayer

The trilayer NCs made with both kinds of the modified heparin (rhodamine-peptide heparin and rhodamine-control peptide heparin) were irradiated with UV light for 2 h using a UV Hand Lamp Spectroline® E-Series UV lamp (output 6 W, wavelength 254 nm). The light source was at 3 cm distance. Photoreaction was conducted without a photoinitiator.

Particle size and Z-potential characterization

The setting parameters for both Particle size and Z-potential measurements were the same as described in chapter 2. All the suspensions were diluted to a droplet concentration of approximately 0.025 (wt%), using Milli-Q water in the case of NE and multilayers terminating with heparin. While the NCs terminating with a chitosan layer were diluted in acidified Milli-Q water solution (pH 4).

Stability tests on crosslinked and not crosslinked trilayers

The stability test of the NCs over time was performed dispersing both the crosslinked and not crosslinked trilayers in different media, i.e. water at pH = 4, PBS 10 mM pH = 7.4. Stability was determined monitoring by DLS particle size variations over time.

Confocal analysis of trilayer nanocapsules

Trilayer on O/W nano-emulsion was diluted 1:25 to a final oil concentration of 0.01 % w/v in an Eppendorf with PBS 10 mM at pH 7.2 and 200 μ l were put in a FD3510 dish for 30 min to allow it to adhere to the surface of the dish. After that, several washes were performed replacing the sample twice with 120 μ l of water. Samples were imaged with a Leica TCS STEDCW microscope (Leica-Microsystems, Mannheim, Germany) equipped with an oil immersion 100 \times objective. Images were acquired with a field of view of 25.6 \times 25.6 μ m for a pixel size of 25 \times 25 nm. The analysis of the images was carried out using LAS AF software.

Cell culture

To test the biological effect of the NCs, human glioma cell line (U87-MG), and primary human dermal fibroblasts (HDF) were used as models of tumor and healthy tissues respectively [20].

HDF cells were cultured in Eagle's minimal essential medium (EMEM) supplemented with 20% Bovine Serum Albumine (FBS, Gibco), 100 U/mL penicillin, 100 mg/mL streptomycin and 2X non-essential aminoacids. U87-MG cells were cultured with EMEM supplemented with 10% FBS and antibiotics.

Both cell lines were maintained in 100 mm diameter cell culture in a humidified controlled atmosphere with 95% to 5% ratio of air/CO₂, at 37 °C. The medium was changed every 2–3 days.

Nanocapsules *in vitro* enzymatic treatment

To observe the effect of the enzymatic cleavage of the NC shell on its drug release and cell-internalization, NCs were treated *in vitro* with 40 nm MMP-2 enzyme. In particular, for cytotoxicity experiments, oil-core NCs were used, while PS core NCs were used for uptake analysis by confocal microscopy.

Before NCs treatment, the enzyme was activated according to the manufacturer's procedure. Briefly, the enzyme (1 Eq) was activated for 3 h at 37 °C by 100 mM APMA solution in Tris–HCl 50 mM, pH 7.2 (45 Eq), at a final enzyme concentrations of 40nM

NCs were then diluted in a MMP-2 buffer solution (50mM HEPES, 200mM NaCl, 10mM CaCl₂, 1mM ZnCl₂, pH 7.4) [19] and incubated for 24h at 37 °C in continuous stirring in presence and absence of the enzyme, to allow the enzymatic degradation of the shell.

For viability test, treated and untreated NCs were diluted in culture medium to a final PXL concentration of 100 nM.

For confocal microscopy imaging, NC suspension was centrifuged at 13,000 rpm for 30 min. Then, the supernatant was carefully removed and collected for further analysis and the NCs were resuspended in cell culture medium by means of an ultrasonic bath (59 Hz, 100% Power, 15 min). The supernatants were then analyzed for Rhod content by a spectrofluorimeter. Samples were read in

triplicate and the linearity of the response was verified over the 0 – 0.065 mM RHOD-PEP concentration range ($r^2 > 0.99$).

Cell viability

Cells were seeded in 96 well microplates at a density of 10^4 cells/well and incubated for 24 h in a humidified atmosphere at 37°C and 5% CO₂ to obtain a subconfluent monolayer.

As already mentioned, for cell viability analysis oil-core nanoparticles were used. In particular, cells were treated with non-functionalized and MMP-2 sensitive NCs which were diluted in culture medium to a final PXL concentration of 100 nM. In both cases enzyme-treated and enzyme-untreated samples were tested. Cells were also treated with cell medium alone as positive control.

The metabolic activity of both cell lines was determined after 24 h and 48 h of exposure by using standard Alamar Blue assay (Life Technologies, Grand Island, NY) according to the manufacturer's procedure. Data represent the cell viability percentage of treated cells normalized to non-treated cells. All the experiments were performed in triplicate.

Confocal microscopy imaging of MMP-2 sensitive nanocapsules in cells

4×10^4 HDF and U87 cells were seeded in 35 mm glass bottom dishes (WillCo-Wells) and incubated for 24 h in a humidified atmosphere at 37°C and 5% CO₂ to obtain a subconfluent monolayer. After that, cells were incubated for 24 h with treated and non-treated PS-core NCs. The samples were the same used for the cytotoxicity assay but in this case the negative control corresponded to uncoated bare PS nanoparticles. Then, samples were washed twice with PBS

to remove non internalized NPs and fixed with paraformaldehyde 4% for 10 min. Finally, cell nuclei were stained with DRAQ5 (Abcam). Samples were observed by confocal multiphoton microscope (Leica TCS SP5 MP, Solms, Germany) with a 25x oil immersion objective. Images were acquired with a resolution of 1024x1024 pixels.

3.6 References

- [1] V.P. Torchilin, Targeted pharmaceutical nanocarriers for cancer therapy and imaging, *Aaps j* 9(2) (2007) E128-47.
- [2] S. Mura, J. Nicolas, P. Couvreur, Stimuli-responsive nanocarriers for drug delivery, *Nature materials* 12(11) (2013) 991-1003.
- [3] J. You, R. Zhang, C. Xiong, M. Zhong, M. Melancon, S. Gupta, A.M. Nick, A.K. Sood, C. Li, Effective photothermal chemotherapy using doxorubicin-loaded gold nanospheres that target EphB4 receptors in tumors, *Cancer research* 72(18) (2012) 4777-86.
- [4] K.J. Chen, H.F. Liang, H.L. Chen, Y. Wang, P.Y. Cheng, H.L. Liu, Y. Xia, H.W. Sung, A thermoresponsive bubble-generating liposomal system for triggering localized extracellular drug delivery, *ACS Nano* 7(1) (2013) 438-46.
- [5] L. Zhang, T. Wang, L. Yang, C. Liu, C. Wang, H. Liu, Y.A. Wang, Z. Su, General route to multifunctional uniform yolk/mesoporous silica shell nanocapsules: a platform for simultaneous cancer-targeted imaging and magnetically guided drug delivery, *Chemistry* 18(39) (2012) 12512-21.
- [6] A. Schroeder, R. Honen, K. Turjeman, A. Gabizon, J. Kost, Y. Barenholz, Ultrasound triggered release of cisplatin from liposomes in murine tumors, *Journal of controlled release : official journal of the Controlled Release Society* 137(1) (2009) 63-8.
- [7] Z. Deng, Z. Zhen, X. Hu, S. Wu, Z. Xu, P.K. Chu, Hollow chitosan-silica nanospheres as pH-sensitive targeted delivery carriers in breast cancer therapy, *Biomaterials* 32(21) (2011) 4976-86.
- [8] A.N. Koo, H.J. Lee, S.E. Kim, J.H. Chang, C. Park, C. Kim, J.H. Park, S.C. Lee, Disulfide-cross-linked PEG-poly(amino acid)s copolymer micelles for glutathione-mediated intracellular drug delivery, *Chemical communications (Cambridge, England)* (48) (2008) 6570-2.
- [9] E. Gullotti, J. Park, Y. Yeo, Polydopamine-based surface modification for the development of peritumorally activatable nanoparticles, *Pharm Res* 30(8) (2013) 1956-67.
- [10] M. Egeblad, Z. Werb, New functions for the matrix metalloproteinases in cancer progression, *Nat Rev Cancer* 2(3) (2002) 161-174.
- [11] G. Klein, E. Vellenga, M.W. Fraaije, W.A. Kamps, E.S. de Bont, The possible role of matrix metalloproteinase (MMP)-2 and MMP-9 in cancer, e.g. acute leukemia, *Critical reviews in oncology/hematology* 50(2) (2004) 87-100.

- [12] L. Zhu, P. Kate, V.P. Torchilin, Matrix metalloprotease 2-responsive multifunctional liposomal nanocarrier for enhanced tumor targeting, *ACS Nano* 6(4) (2012) 3491-8.
- [13] T. Terada, M. Iwai, S. Kawakami, F. Yamashita, M. Hashida, Novel PEG-matrix metalloproteinase-2 cleavable peptide-lipid containing galactosylated liposomes for hepatocellular carcinoma-selective targeting, *Journal of controlled release : official journal of the Controlled Release Society* 111(3) (2006) 333-42.
- [14] V. Calcagno, R. Vecchione, A. Sagliano, A. Carella, D. Guarnieri, V. Belli, L. Raiola, A. Roviello, P.A. Netti, Biostability enhancement of oil core - polysaccharide multilayer shell via photoinitiator free thiol-ene 'click' reaction, *Colloids and surfaces. B, Biointerfaces* 142 (2016) 281-9.
- [15] M.T. Basel, T.B. Shrestha, D.L. Troyer, S.H. Bossmann, Protease-sensitive, polymer-caged liposomes: a method for making highly targeted liposomes using triggered release, *ACS Nano* 5(3) (2011) 2162-75.
- [16] G. Decher, Fuzzy Nanoassemblies: Toward Layered Polymeric Multicomposites, *Science (New York, N.Y.)* 277(5330) (1997) 1232-1237.
- [17] C.E. Hoyle, C.N. Bowman, Thiol-ene click chemistry, *Angew Chem Int Ed Engl* 49(9) (2010) 1540-73.
- [18] G.K. Such, E. Tjipto, A. Postma, A.P. Johnston, F. Caruso, Ultrathin, responsive polymer click capsules, *Nano Lett* 7(6) (2007) 1706-10.
- [19] D. Guarnieri, M. Biondi, H. Yu, V. Belli, A.P. Falanga, M. Cantisani, S. Galdiero, P.A. Netti, Tumor-activated prodrug (TAP)-conjugated nanoparticles with cleavable domains for safe doxorubicin delivery, *Biotechnol Bioeng* 112(3) (2015) 601-11.
- [20] M. Cantisani, D. Guarnieri, M. Biondi, V. Belli, M. Profeta, L. Raiola, P.A. Netti, Biocompatible nanoparticles sensing the matrix metalloproteinase 2 for the on-demand release of anticancer drugs in 3D tumor spheroids, *Colloids and surfaces. B, Biointerfaces* 135 (2015) 707-16.
- [21] V. Calcagno, R. Vecchione, A. Sagliano, A. Carella, D. Guarnieri, V. Belli, L. Raiola, A. Roviello, P.A. Netti, Biostability enhancement of oil core—polysaccharide multilayer shell via photoinitiator free thiol-ene 'click' reaction, *Colloids and Surfaces B: Biointerfaces* 142 (2016) 281-289.

Chapter 4

Graphene oxide oil-core nanocapsules

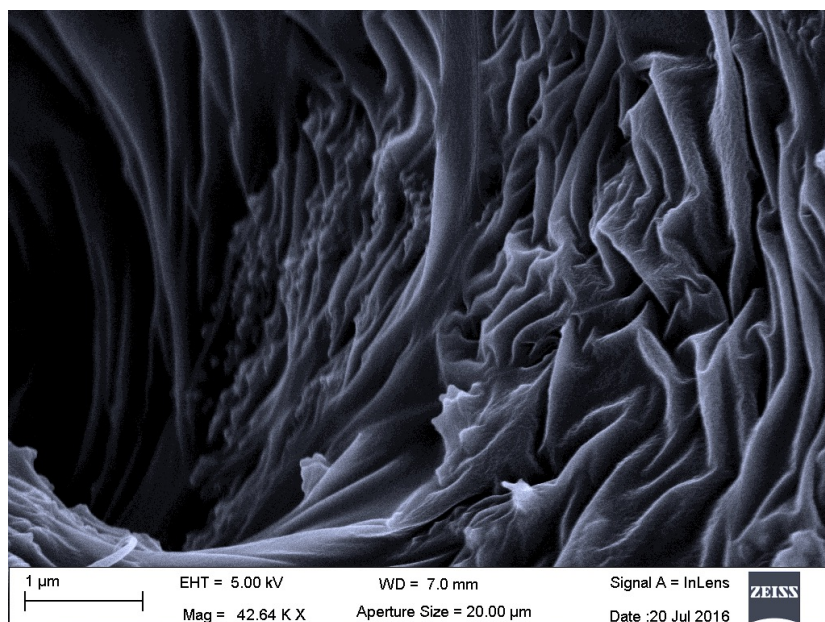


Figure 4.1.1 A scanning electron microscope image of a drop of graphene oxide after freeze-drying process.

Abstract

Graphene oxide (GO) is gradually breaking the taboo of its application into the biomedical field. The outstanding optical properties and the unparalleled loading capacity make GO a key nanomaterial for several medicine and biotechnology offshoots ranging from bioimaging to *stimuli* responsive drug delivery and photo-thermal therapy. However, combining all these intriguing features into a multimodal therapeutic platform still proves challenging. To this aim, very little has been done for the integration of GO into nanosized drug delivery systems and the only relevant cases deal with the Layer-by-Layer deposition of GO on sacrificial template microcapsules. Moving from these considerations, here we report on some preliminary results we achieved starting from commercially available GO together with a robust platform for the preparation of ultrastable liquid nanocapsules. First we chemically and mechanically treated GO to obtain fluorescent nanosheets, which we then integrated onto monodisperse O/W nanoemulsions by facile LbL technique. This way we prepared GO coated nanocapsules that we preloaded with a chemotherapeutic agent. When incubated with two cell lines (healthy and tumor) the NCs showed strong non-linear fluorescence in the cell nuclear region under two-photon excitation. These results unfold some interesting scenarios including the chance to track the fate of the drug delivery system after its administration.

4.1 Introduction

Why is there so much noise around the word graphene? What does it make this relatively young material so special to a certain research community eyes, while some others stay skeptical and do not actually feel the hype?

Whatever your stance, graphene has already invaded virtually every nanotechnology offshoots, with uncountable potential applications inching their way into a near-future marketplace.

At a first glance, probably most of the paradigm-shifting fascination attributed to graphene depends on its condensed matter: it is the first two-dimensional material that has been physically isolated! Its name, indeed, is referred to a flat monolayer of sp^2 -hybridized carbon atoms tightly packed into a honeycomb lattice. Although scientists were theorizing about one atom thick, two-dimensional crystals since 1970s, freestanding graphene was presumed not to exist mainly due to thermodynamic instability. Thereby, its finding by Novoselov and Geim in 2004 [1, 2] suddenly disclosed all its potential, also paving the way for other two-dimensional crystals (*i.e.* phosphorene [3], germanene [4], silicene [5] and so on). The unique nature of its charge carriers [6, 7] and their interaction with the crystal lattice is mainly responsible for the huge deal of research interest. A deep understanding and fine control of graphene zero-band gap electronic structure (see **Figure 4.1.2**) and ballistic conduction could actually open up new opportunities in several key technological fields and also contribute to the development of a novel platform with important social and economic impacts.

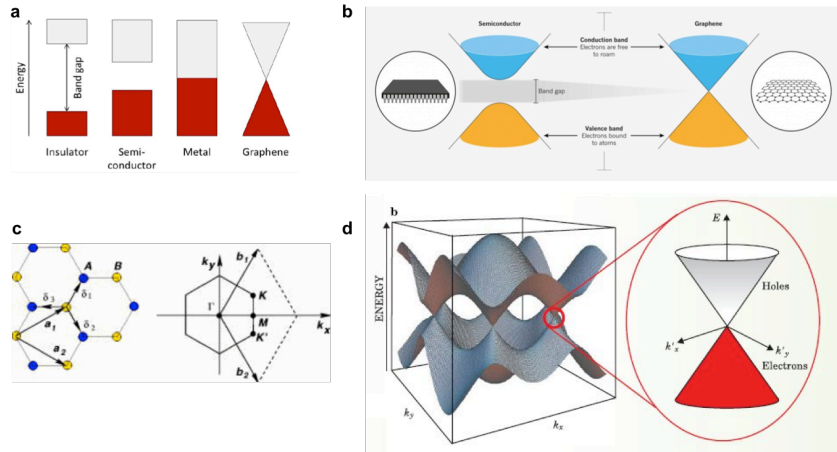


Figure 4.1.2 Mind the Gap! (a) Classification of materials based on their conductive properties and relative energy band gap. (b) Distinction between semiconductors and graphene behavior highlighting the almost zero band gap of the latter. (c) Left: lattice structure of graphene. Right: corresponding Brillouin zone. (d) Graphene band structure and a zoom in of the energy bands close to one of the Dirac points. (Figures readapted from: (a) <http://www.azonano.com/article.aspx?ArticleID=4264>; (b) <http://nauka.in.ua/upload/medialibrary/651/651c83f718b2a807c335d2cbbf396a96.jpg>; (c) ref. [7]; (d) <http://www.th.u-psud.fr/>).

Among the most mind-blowing opportunities potentially enabled by technological translation of graphene intriguing properties, there are stretchable electronics (flexible and wearable devices), ultrasensitive sensors, high frequency devices (THz), and ultradense data storage (for more examples see **Table 4.1.1**).

Table 4.1.1 A schematic correlation between graphene properties and their possible technological conversion with relative impact on society. (Table readapted from ref [8]).

| features | enabled application/technologies | impact |
|--|--|---|
| atomic thinness | flexible devices; thin and flexible electronic components; modular assembly/distribution of portable thin devices | spectrum of new forms of devices, thus enabling new concepts of integration and distribution |
| foldable materials | engineering new materials by stacking different atomic planes or by varying the stacking order of homogeneous atomic planes | |
| all-surface material | engineering novel 2d crystal with tunable physical/chemical properties by control of the surface chemistry. Platform for new chemical/biological sensors | development of new materials which properties could be engineered and customized for new applications |
| solution - processable | novel composite materials with outstanding physical properties (e.g. high thermal conductivity, high Young modulus and tensile strength); novel functional materials | |
| high carrier mobility (μ) | ultra-high frequency electronic devices | new highly-performing devices available at low cost and large scale, thus allowing major step forwards in many social impact fields (e.g. environmental monitoring, communications, health / medical applications, etc) |
| optical (saturable) absorption; photo-thermoelectric effect | novel optoelectronic and thermoelectric devices; photodetectors | |
| field-effect sensitivity | highly sensitive transducers | |
| high intrinsic capacitance; high specific surface area | outstanding supercapacitors | significant steps forward in the production of sustainable devices and green-energy systems |
| photovoltaic effect, broad-range transparency; photocatalytic effect | energy conversion; energy harvesting; self-powered devices | |
| theoretically predicted "chiral superconductivity" | high Tc superconductors | new devices based on yet experimentally unexplored physics |
| Dirac fermions; pseudospin | valleytronics | |

More recently, the chemically derived forms of graphene have also received much attention, especially graphene oxide (GO) due to several advantages, not least the preferred routes for a large-scale manufacturing. Indeed, a viable way to produce graphene materials is by chemical exfoliation of graphite under strong oxidizing conditions [9, 10]. This way in GO, the 100% sp^2 two-dimensional network of pristine graphene becomes a mixture of sp^2 and sp^3 bonded carbon atoms. In particular, the oxygen defects within graphene surface are introduced in the form of epoxy and hydroxyl groups covalently bonded with the sp^3 hybridized carbon atoms. Whereas, the remaining fraction of sp^2 hybridized carbon atoms are bonded either with neighboring carbon atoms or with oxygen in the form of carboxyl and carbonyl groups. The latters are located

mostly at the edges of the GO sheets (see **Figure 4.1.3** for a schematic representation). As a first consequence, the presence of these functional groups within GO sheets make it hydrophilic thus allowing its dispersion in water [11], in contrast to pristine graphene. This prerogative combined to the outstanding optoelectronic and photothermal properties arising from GO unique heterogeneous atomic and electronic structure, is breaking the taboo of studying graphene-derived materials for nanomedicine and biotechnology applications [12, 13].

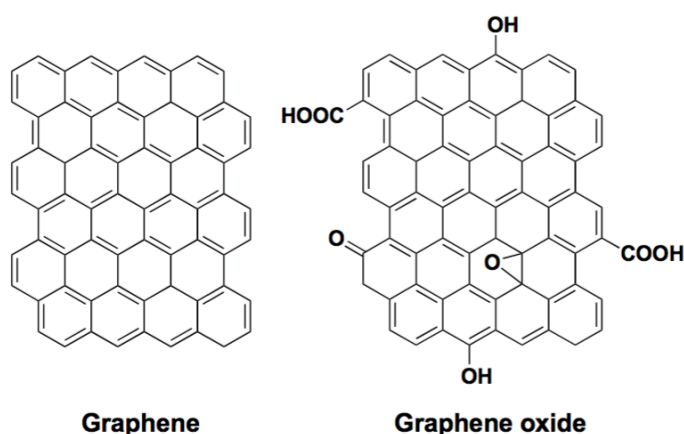


Figure 4.1.3 The structures of graphene and graphene oxide (Figure redrawn after ref [12]).

Of course, the use of carbon nanomaterials in the biomedical field has raised much of debate mainly due to safety issues. Several cytotoxicity studies revealed many possible mechanisms induced by GO including hemolytic activity [14], cell starvation [15], generation of reactive oxygen species (ROS) and apoptosis [16]. On the other hand, there are examples where by means of PEGylation and a lower graphene dose, no significant toxic effects are observed on the long term [17]. True is that the current stage of research on toxicity of GO is still in its infancy and the relevant data are rather scattered. In the meanwhile, all the potential GO shows in the biomedical research area keeps on legitimize its

investigation. In particular, its huge surface area disseminated with aromatic rings enables high loading of hydrophobic molecules simply by van der Waals or $\pi - \pi$ interactions, thus making GO an ideal candidate for the delivery of water-insoluble aromatic anticancer drugs [18].

Another appealing feature of GO for nanomedicine is its strong optical absorption in the near-infrared (NIR) region of light (700-900 nm), which is a tissue transparency window ideal for optical imaging and phototherapies. The heat generated by GO upon irradiation, indeed, can be exploited in cancer therapy for hyperthermia treatment [19] as well to trigger drug release from heat responsive nanocarriers [20].

Furthermore, GO broad fluorescence has been lately highlighted and investigated. Several works have shown that the fluorescence of GO can be observed and tuned by modifying the content of oxygen-containing groups or by reducing its size to the nanometer scale [11, 21-25]. However, it is noteworthy that most of this research is focused on the luminescence induced by continuous-wave lasers through one-photon excitation and with emission in the near-UV/visible band. Whereas, only few papers report on two- or multi-photon fluorescence induced with a NIR laser [26-28], which is of real interest for nanomedicine and biotechnology applications. This microscopy technique, indeed, allows for reduced photobleaching and phototoxicity, minimized tissue auto-fluorescence background, and deep tissue penetration as a consequence of low Rayleigh scattering and low tissue absorption of NIR light [29]. True is that due to the strong heterogeneity of GO atomic and electronic structure there is still a lack of knowledge around the origin of its fluorescence. What is clear is that GO nanosheets are a mixture of sp^2 and sp^3 domains where sp^2 nanoislands are immersed and localized in an sp^3 matrix. Therefore, one of the most accepted explanations sees fluorescence arising from the electrons/holes recombination as a consequence of a quantum confinement effect [4, 21] (see **Figure 4.1.4** for a schematic representation).

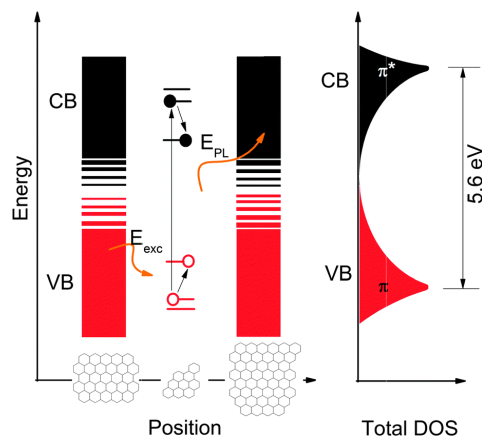


Figure 4.1.4 Schematic band structure of GO. Smaller sp² domains have a larger energy gap due to a stronger confinement effect. DOS - electronic density of states. (Figure redrawn after ref. [11]).

Doing the math on what has just been outlined about graphene and especially GO, several appealing features appear to project these materials toward powerful biotechnological applications. However, in order to draw fully from graphene/GO it is imperative to exhaustively reveal their chemistry and physics as well as their interaction with biology. On the other hand, this lack of knowledge leaves some room for yet unexploited research areas.

In light of the above, here we started to explore some of the GO potential for drug delivery. In particular, based on a robust platform for the preparation of LbL lipid NCs, we tried to add GO nanosheets on our delivery systems. To this aim, very little has been done for the integration of GO nanosheets with nanosized drug delivery systems. To the best of our knowledge, the only relevant cases deal with the LbL deposition of GO on sacrificial template microcapsules [30-32]. Thus, the first real objective of this work was coating nanosized liquid templates with GO. This step required manipulation and following analysis of the commercially available GO in order to allow for its LbL deposition on our NEs. The GO multilayer NCs were characterized by

DLS and cryo-TEM. Moreover, they showed strong fluorescent emission in the visible region of light under two-photon excitation.

4.2 Results and Discussion

Graphene oxide modification and its deposition on O/W nanoemulsions

When we tried to deposit a suspension of these GO sheets on our NEs, the LbL process did lead to a complete aggregation of the system. Thereby, we first tried to get insight on the size distribution of the GO suspension. The cryo-TEM image in **Figure 4.2.1** reveals the average dimensions of the commercial GO, as it was supplied from the manufacturing company. Based on the experience matured on our system, an increase in GO Z-potential (absolute value) and a reduction of the sheets size were auspicated to achieve the LbL deposition of a GO layer around the nanosized liquid templates.

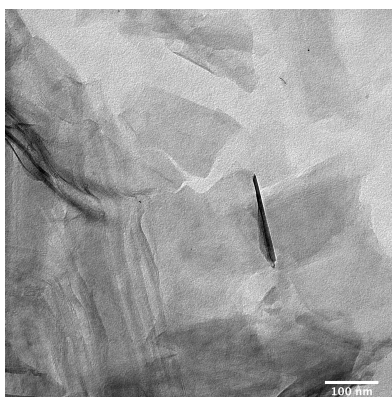


Figure 4.2.1 Cryo-TEM image of GO as supplied from the company manufacturer (Sigma Aldrich). (Scale bar 100 nm).

Following this aim, we chemically treated the commercial GO converting the oxydril groups into carboxylic acids as highlighted by the X-rays photoelectron spectroscopy (XPS) analysis. **Figure 4.2.1** shows the high resolution C1s XPS spectra for pristine GO (a) and treated GO (b). Six components have been fitted for each sample with Gaussian peaks centered at 284.7, 284.88, 286.78,

287.49, 288.60 and 290.53 eV corresponding to C=C, C-C, C-O, C=O, COOH and $\pi - \pi^*$. Minor (0.1 – 0.5 eV) shift/error in the binding energies were detected between the pristine and treated spectra. The contribution of each individual functional group is shown in the figure legends. Comparing the two samples it is clear how the C-O contribution dramatically decreases in treated GO, while the COOH increases. These results confirmed that the chemical treatment with chloroacetic acid effectively determined a certain degree of carboxylation of GO. At the same time, the treated GO XPS spectrum also showed an increase of C=C contribution which may be indicative of a partial restoration of sp^2 domains. These results combined with the UV spectra in **Figure 4.2.2** suggest that the increase in the concentration of sp^2 hybridized carbon atoms partially restored a graphene-like nature. The red shift of main absorption peak of treated GO to 265 nm and the increase of absorption in the whole spectral region indicate that $\pi - \pi^*$ transitions of C=C are dominant on $n - \pi^*$ of the C=O. These results are consistent with the typical UV spectra obtained after weak reduction process as reported in ref. [32].

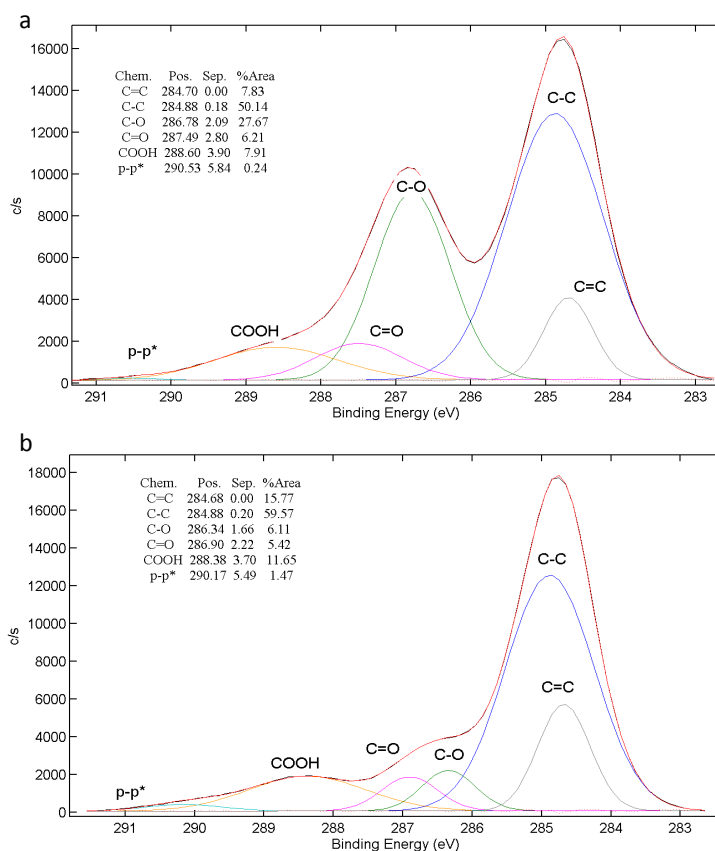


Figure 4.2.2 C1s XPS spectra for pristine GO (a) and treated GO (b).

To explain this combined effect of partial oxidation of GO on one side, and a certain degree of reduction to sp^2 carbon atoms on the other side, we formulated the following hypothesis: the chemical treatment of GO with chloroacetic acid was responsible for a partial oxidation of C-OH to $-COOH$ groups. At the same time, the sonication of GO under alkaline conditions and slight increasing temperature - due to dissipation of energy - led to an increase of sp^2 domains. In particular, the higher concentration of C=C groups apparently might be attributed to partial removing of carbonaceous oxidation debris from GO [33]. This low molecular weight fraction, made of a bunch of oxidative polyaromatic fragments, has been found to strongly adsorbed on GO by non-covalent interactions acting as a lubricant among the sheets [33, 34].

Therefore, in spite of a proper reduction process, which for GO is generally reported to take place under strong alkaline conditions (as in case of hydrazine reduction [35]), here we assume that the increase of the C=C contribution actually depends on the proportional decrease of the C=O components after base-washing during the sonication process.

It is noteworthy that a good compromise between the oxidized and reduced GO form is crucial in order to preserve water dispersion ability and the non-zero energy band gap.

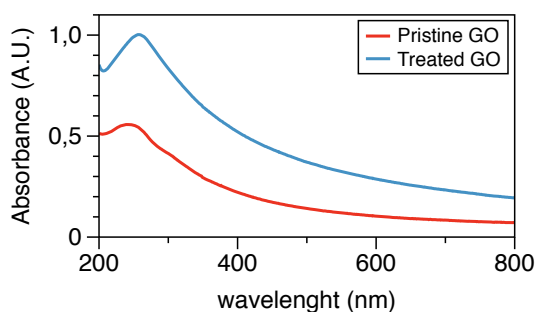


Figure 4.2.3 UV-visible spectra of GO before and after chemical/thermo-mechanical treatment.

The size decrease of GO sheets after treatment is pretty evident from **Figure 4.2.4** comparing the cryo-TEM images of GO before (**Fig. 4.2.4a**) and after sonication (**Fig. 4.2.4b**).

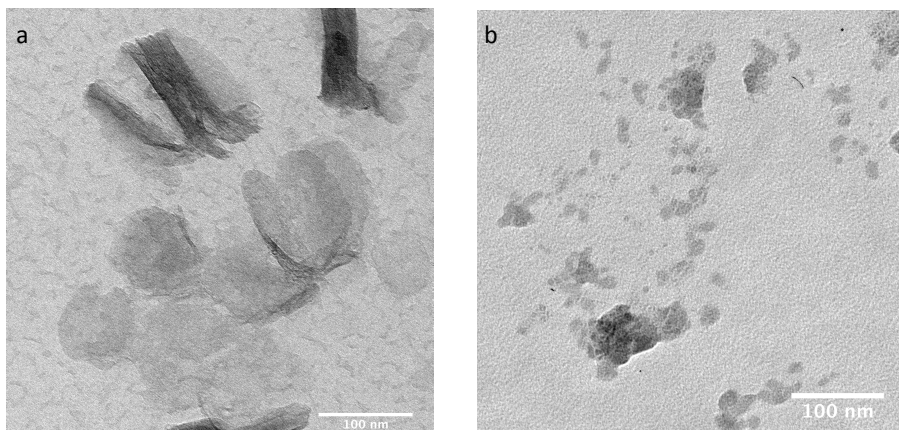


Figure 4.2.4 Cryo TEM images of GO before (a) and after (b) sonication. (Scale bar: 100nm).

The as prepared GO was then assembled around 2% v/v O/W NEs thanks to a LbL procedure allowing for a high control over the deposition process, as already described elsewhere (see chapters 2 and 3 and ref [36]). Due to the nanoscale size of the templates and to their liquid state, performing the LbL of GO nanosheets was not straightforward. The same applies for morphology, although from cryo-TEM images in **Figure 4.2.5** (b,d) the formation of GO coating around the NE template is pretty evident. Following this procedure, we deposited on NEs two layers of negatively charged GO alternated to positively charged chitosan. We monitored the evolution of the NCs from the starting NE until the formation of a tetralayer by DLS and the average values of size PDI and Z-potential are summarized in **Figure 4.2.5**.

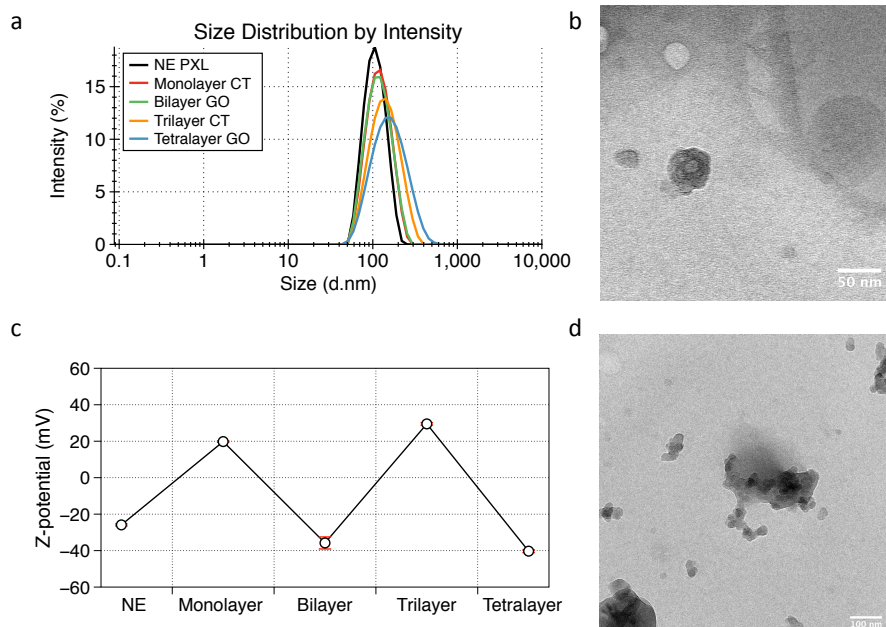


Figure 4.2.5 Characterization of GO multilayer NCs during LbL deposition process by (a) DLS, (b) and (d) cryo-TEM, (c) Z-potential. (Scale bar: 100 nm).

The GO tetralayer NCs were also observed at the multi-photon confocal microscope. When excited between 700 and 960 nm they showed an intense fluorescence emission over the visible region of wavelengths (**Figure 4.2.6b**). Usually, photosensitizers absorb light in the visible spectral region below 700 nm, where light penetration into the tissue is limited and one-photon absorption induced auto-fluorescence is higher. Whereas, the 700–900 nm wavelength range is typically recognized as a main optical transparent window for tissues, as Rayleigh scattering is very low. Therefore, two-photon luminescence microscopy making use of NIR femtosecond excitation source is highly demanded for bioimaging applications.

Although GO fluorescence has been already described and debated, there are only few examples reporting two-photon induced emission. Encouraged by the non-trivial optical response of our system we further investigated GO NCs luminescence by *in vitro* live imaging. After 24 h of incubation with both human

primary glioblastoma (U87) and primary human dermal fibroblasts (HDF) cells, GO NCs were taken up and showed intense fluorescence signal (**Figure 4.2.7**). No significant changes were observed when the wavelength was varied between 780 nm and 900 nm even at the very low laser power. It is noteworthy that a two-photon molecular dye exhibiting a photoluminescence that can be excited with a wider range of wavelengths is itself of practical significance in bioimaging. These preliminary results allowed for highly cyto-compatible imaging conditions paving the way to a new set of *in vitro* experiments.

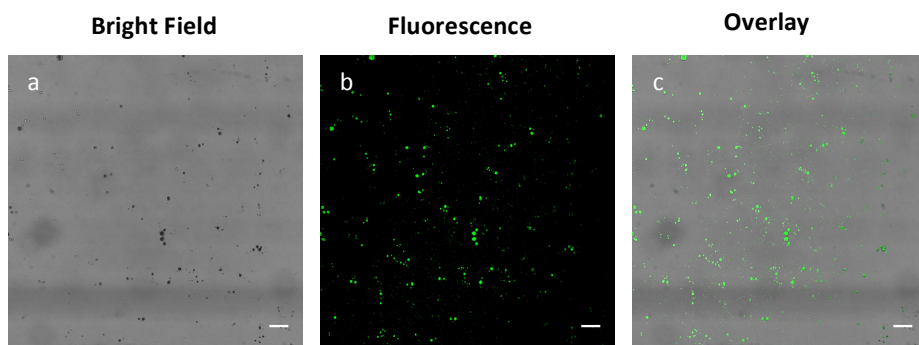


Figure 4.2.6 Multi-photon microscope images of GO NCs in bright field (a), fluorescence (b), and their overlay (c). (Scale bar: 10 μm).

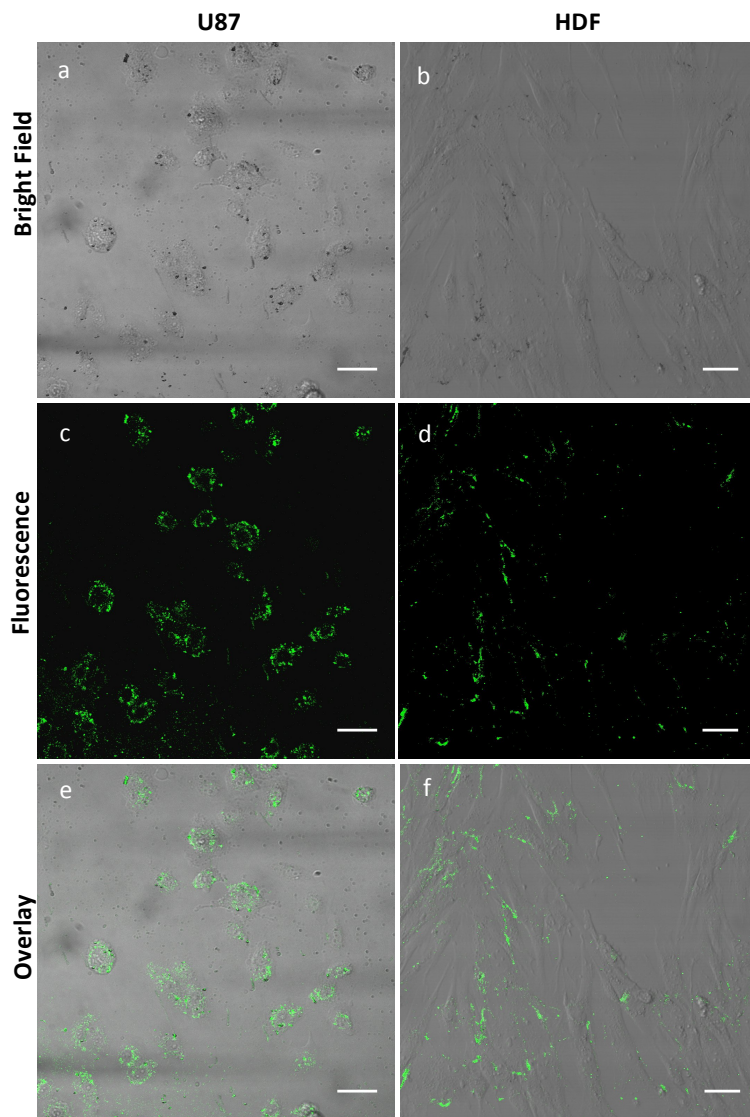


Figure 4.2.7 Multiphoton confocal microscope images of tetralayer GO/CT NCs after internalization in both U87 and HDF cells. a, b: bright field images; c, d: multiphoton fluorescence images; e, f: overlay of bright field and multiphoton fluorescence images. (Scale bar: 40 μm).

4.3 Conclusions

The main ambition of this work was trying to assemble few atoms-thick GO sheets on oil-core NCs in order to develop an innovative drug delivery platform. Although GO deserves deeper understanding as a material itself, it has already disclosed part of its great potential in the biomedical field. Among the many remarkable feature of GO, drug delivery would particularly benefit from the unparalleled loading capacity of hydrophobic molecules, the multi-photon induced luminescence and the ability to transduce NIR light into heat. So far the only examples where GO has been integrated into drug delivery systems involves the use of microcapsules and stand-alone GO. Encouraged by the non conventional opportunities GO promises to offer, we successfully built GO multilayer NCs combining an effective chemical/structural modification of the material with a robust technique for the preparation of oil-core multilayer NCs. To confirm the quality of the system we provided spectroscopic, dimensional and morphological evidences. Moreover, the GO NCs showed a powerful two-photon fluorescence that incentivized further study for bioimaging applications. Preliminary *in vitro* imaging experiments highlighted a massive uptake by two different cell lines through the intense fluorescence of GO NCs over a broad band of wavelengths. These results unfold some interesting scenarios including the chance to track the fate of the drug delivery system after its administration.

4.4 Future Perspectives

Based on the photo-thermal properties reported on GO, we are currently exploring the ability of GO NCs to transduce the NIR light into heat. This prerogative could enable our system for a double therapeutic approach. The heat generated under biocompatible wavelengths, indeed, might both induce tumor cell death by hyperthermia and trigger the release of an anticancer drug from the NCs. By coupling these two effects, indeed, one could benefit from the photo-thermal therapeutic approach on the short time scale, while the *stimuli* responsive drug delivery system may exert its action on a longer time scale.

As a future prospective we will thus devote some efforts to further study GO optical properties with the ambition of combining its intriguing features into a graphene-based multimodal therapeutic platform of real interest for nanomedicine.

4.5 Materials and Methods

Materials

O/W NEs were prepared using Soybean oil (density of 0.922 g/ml at 20 °C) and surfactant Lipoid E80 (egg lecithin powder 80-85% enriched with Phosphatidyl choline (PC) and 7-9.5% content in phosphatidyl ethanolamine (PE)) purchased from Lipoid and used without further purification. Millipore[®] Milli-Q water was used for the preparation of all NEs and solutions. Chloroacetic acid (ClCH_2COOH m.w. = 94.5 g/mol), Sodium hydroxide (NaOH m.w. = 40.0 g/mol), (CT, LMW 90-150 kDa, DDA 84% determined via $^1\text{H-NMR}$) and graphene oxide water suspension (GO 2 mg/ml) were purchased from Sigma Aldrich.

Oil-in-Water nanoemulsion

The O/W NE was prepared as previously described (see chapter 2). Briefly, the oil phase was prepared by adding an exact amount of Lipoid E 80 to the soy-bean oil at 60 °C and then sonicated with an immersion sonicator (Ultrasonic Processor VCX500 Sonic and Materials). To obtain the pre-emulsion, the oil phase was added dropwise to a weighted amount of aqueous phase (Milli-Q water) and mixed using the immersion sonicator. The pre-emulsion was finally passed at 2000 bar through the high-pressure valve homogenizer (Microfluidics M110PS) to obtain the final NE.

Chemical and structural modification of graphene oxide

Commercial GO was chemically modified based on a procedure described elsewhere [22]. In order to convert -OH groups into -COOH, 10 ml of graphene oxide water suspension (GO 2 mg/ml) was diluted to 0.05 mg/ml with Milli-Q water and sonicated for one hour. Then, 30 mg of NaOH plus 25 mg of ClCH₂COOH were added to the suspension and bath sonicated for other 2 hours. The suspension was also thermo-mechanically treated with an immersion sonicator for an extra hour. Afterwards, the reaction mixture was neutralized with HCl and washed several times with Milli-Q. The carboxylated GO was finally freeze-dried and stored in dry conditions ready to use.

LbL deposition of modified graphene oxide on O/W nanoemulsions

Monolayer, bilayer, trilayer and tetralayer were obtained with a customized LbL deposition procedure [36] already reported in chapter 2 and 3. Briefly, the tetralayer NCs were prepared by aid of two syringe pumps (HARVARD APPARATUS 11 PLUS) and an ultrasonic bath (FALC INSTRUMENTS). Starting from the chitosan coated NE (1 wt% oil and 0.01 wt% chitosan), a negatively charged second GO layer was deposited by mixing 1 : 1 (v : v) of a 0.1 wt% aqueous solution of GO with the NE suspension. The same procedure was repeated also for the deposition of the subsequent chitosan and GO layers leading to the following final concentrations: 0.0125 % (w/v) O/W NE, 0.002 % (w/v) CT, 0.0263 % (w/v) GO.

Particle size and Z-potential measurements

The setting parameters for both Particle size and Z-potential measurements were the same as described in chapter 2. All the suspensions were diluted to a droplet concentration of approximately 0.025 (wt%), using Milli-Q water in the case of nano-emulsion and multilayers terminating with GO, while the NCs terminating with a chitosan layer were diluted in acidified Milli-Q water solution (pH 4).

XPS analysis

XPS spectra were recorded using a PHI5000VersaProbeII XPS spectrometer with a monochromatic Al-K- α source of 1486.68 eV. The high resolution C1s spectra were acquired at high power (100 W) with a Pass Energy of 23.5 eV, 0.1 eV step size, and averaged over 20 scans. Spectra from insulating samples were charged corrected by shifting all peaks to the adventitious carbon C1s spectral component binding energy set at 284.8 eV. Multipack software was used to process all the spectra.

Cryo-TEM analysis

The morphology of the NEs and multilayer NCs were observed by cryo-TEM. In particular, frozen hydrated samples were prepared by applying a 3 μ l aliquot to a previously glow-discharged 200 mesh holey carbon grid (Ted Pella, USA). Before plunging into nitrogen cooled liquid ethane, the grid was blotted for 1.5 s in a chamber at 4 °C and 90% humidity using a FEI Vitrobot Mark IV (FEI company, the

Netherlands). The particles were imaged using a Tecnai G2 F20 transmission electron microscope (FEI company, the Netherlands) equipped with a Shotky field emission gun operating at an acceleration voltage of 200 kV and recorded at low dose with a 2k x 2k Ultrascan (Gatan, USA) CCD camera.

Cell culture and sample preparation

To test the biological effect of GO NCs, human glioma cell line (U87-MG), and primary human dermal fibroblasts (HDF) were used as models of tumor and healthy tissues respectively.

HDF cells were cultured in Eagle's minimal essential medium (EMEM) supplemented with 20% Bovine Serum Albumine (FBS, Gibco), 100 U/mL penicillin, and 100 mg/ml streptomycin and 2X non-essential aminoacids. U87-MG cells were cultured with EMEM supplemented with 10% FBS and antibiotics.

Both cell lines were maintained in 100 mm diameter cell culture in a humidified controlled atmosphere with 95% to 5% ratio of air/CO₂, at 37 °C. The medium was changed every 2–3 days.

For Imaging experiments, 4×10^4 HDF and U87 cells were seeded in 35mm glass bottom dishes (WillCo-Wells) and incubated for 24 h in a humidified atmosphere at 37 °C and 5% CO₂ to obtain a subconfluent monolayer. After that, cells were incubated for 24 h with GO NCs. Then, samples were washed twice with PBS to remove non internalized NPs and cell medium was added.

GO nanocapsules imaging in living cells

Samples were observed by LSM microscope system (Leica TCS SP5 II) equipped with multiphoton module based on a Ti sapphire NIR coherent laser (Chameleon ultra II). A water-immersion 40x/1.1 objective was used to acquire images of living cells, using 800 nm as excitation wavelength at very low laser power. Images were acquired with a resolution of 1024x1024 pixels.

4.6 References

- [1] K.S. Novoselov, A.K. Geim, S.V. Morozov, D. Jiang, Y. Zhang, S.V. Dubonos, I.V. Grigorieva, A.A. Firsov, Electric Field Effect in Atomically Thin Carbon Films, *Science* (New York, N.Y.) 306(5696) (2004) 666-669.
- [2] K.S. Novoselov, D. Jiang, F. Schedin, T.J. Booth, V.V. Khotkevich, S.V. Morozov, A.K. Geim, Two-dimensional atomic crystals, *Proceedings of the National Academy of Sciences of the United States of America* 102(30) (2005) 10451-3.
- [3] H. Liu, A.T. Neal, Z. Zhu, Z. Luo, X. Xu, D. Tomanek, P.D. Ye, Phosphorene: an unexplored 2D semiconductor with a high hole mobility, *ACS Nano* 8(4) (2014) 4033-41.
- [4] C.C. Liu, W. Feng, Y. Yao, Quantum spin Hall effect in silicene and two-dimensional germanium, *Physical review letters* 107(7) (2011) 076802.
- [5] T. Osaka, H. Omi, K. Yamamoto, A. Ohtake, Surface phase transition and interface interaction in the α -Sn/InSb{111} system, *Physical review. B, Condensed matter* 50(11) (1994) 7567-7572.
- [6] A.K. Geim, K.S. Novoselov, The rise of graphene, *Nature materials* 6(3) (2007) 183-191.
- [7] A.H. Castro Neto, F. Guinea, N.M.R. Peres, K.S. Novoselov, A.K. Geim, The electronic properties of graphene, *Reviews of Modern Physics* 81(1) (2009) 109-162.
- [8] A.C. Ferrari, F. Bonaccorso, V. Fal'ko, K.S. Novoselov, S. Roche, P. Boggild, S. Borini, F.H. Koppens, V. Palermo, N. Pugno, J.A. Garrido, R. Sordan, A. Bianco, L. Ballerini, M. Prato, E. Lidorikis, J. Kivioja, C. Marinelli, T. Ryhanen, A. Morpurgo, J.N. Coleman, V. Nicolosi, L. Colombo, A. Fert, M. Garcia-Hernandez, A. Bachtold, G.F. Schneider, F. Guinea, C. Dekker, M. Barbone, Z. Sun, C. Galiotis, A.N. Grigorenko, G. Konstantatos, A. Kis, M. Katsnelson, L. Vandersypen, A. Loiseau, V. Morandi, D. Neumaier, E. Treossi, V. Pellegrini, M. Polini, A. Tredicucci, G.M. Williams, B.H. Hong, J.H. Ahn, J.M. Kim, H. Zirath, B.J. van Wees, H. van der Zant, L. Occhipinti, A. Di Matteo, I.A. Kinloch, T. Seyller, E. Quesnel, X. Feng, K. Teo, N. Rupesinghe, P. Hakonen, S.R. Neil, Q. Tannock, T. Lofwander, J. Kinaret, Science and technology roadmap for graphene, related two-dimensional crystals, and hybrid systems, *Nanoscale* 7(11) (2015) 4598-810.
- [9] W.S. Hummers, R.E. Offeman, Preparation of Graphitic Oxide, *Journal of the American Chemical Society* 80(6) (1958) 1339-1339.
- [10] R. Ruoff, Graphene: Calling all chemists, *Nat Nano* 3(1) (2008) 10-11.
- [11] G. Eda, Y.-Y. Lin, C. Mattevi, H. Yamaguchi, H.-A. Chen, I.S. Chen, C.-W. Chen, M. Chhowalla, Blue Photoluminescence from Chemically Derived Graphene Oxide, *Advanced Materials* 22(4) (2010) 505-509.

- [12] X. Zhou, F. Liang, Application of Graphene/Graphene Oxide in Biomedicine and Biotechnology, *Current Medicinal Chemistry* 21(7) (2014) 855-869.
- [13] D. Bitounis, H. Ali-Boucetta, B.H. Hong, D.H. Min, K. Kostarelos, Prospects and challenges of graphene in biomedical applications, *Adv Mater* 25(16) (2013) 2258-68.
- [14] K.-H. Liao, Y.-S. Lin, C.W. Macosko, C.L. Haynes, Cytotoxicity of graphene oxide and graphene in human erythrocytes and skin fibroblasts, *ACS applied materials & interfaces* 3(7) (2011) 2607-2615.
- [15] L. Guo, A. Von Dem Bussche, M. Buechner, A. Yan, A.B. Kane, R.H. Hurt, Adsorption of Essential Micronutrients by Carbon Nanotubes and the Implications for Nanotoxicity Testing, *Small (Weinheim an der Bergstrasse, Germany)* 4(6) (2008) 721-727.
- [16] Y. Zhang, S.F. Ali, E. Dervishi, Y. Xu, Z. Li, D. Casciano, A.S. Biris, Cytotoxicity effects of graphene and single-wall carbon nanotubes in neural phaeochromocytoma-derived PC12 cells, *ACS Nano* 4(6) (2010) 3181-6.
- [17] K. Yang, J. Wan, S. Zhang, Y. Zhang, S.T. Lee, Z. Liu, In vivo pharmacokinetics, long-term biodistribution, and toxicology of PEGylated graphene in mice, *ACS Nano* 5(1) (2011) 516-22.
- [18] Z. Liu, J.T. Robinson, X. Sun, H. Dai, PEGylated Nanographene Oxide for Delivery of Water-Insoluble Cancer Drugs, *Journal of the American Chemical Society* 130(33) (2008) 10876-10877.
- [19] K. Yang, S. Zhang, G. Zhang, X. Sun, S.-T. Lee, Z. Liu, Graphene in Mice: Ultrahigh In Vivo Tumor Uptake and Efficient Photothermal Therapy, *Nano Letters* 10(9) (2010) 3318-3323.
- [20] S. Mura, J. Nicolas, P. Couvreur, Stimuli-responsive nanocarriers for drug delivery, *Nature materials* 12(11) (2013) 991-1003.
- [21] S. Vempati, T. Uyar, Fluorescence from graphene oxide and the influence of ionic, pi-pi interactions and heterointerfaces: electron or energy transfer dynamics, *Phys Chem Chem Phys* 16(39) (2014) 21183-203.
- [22] X. Sun, Z. Liu, K. Welscher, J.T. Robinson, A. Goodwin, S. Zaric, H. Dai, Nano-Graphene Oxide for Cellular Imaging and Drug Delivery, *Nano research* 1(3) (2008) 203-212.
- [23] Z. Luo, P.M. Vora, E.J. Mele, A.C. Johnson, J.M. Kikkawa, Photoluminescence and band gap modulation in graphene oxide, *Applied physics letters* 94(11) (2009) 111909.
- [24] T. Gokus, R.R. Nair, A. Bonetti, M. Bohmler, A. Lombardo, K.S. Novoselov, A.K. Geim, A.C. Ferrari, A. Hartschuh, Making graphene luminescent by oxygen plasma treatment, *ACS Nano* 3(12) (2009) 3963-8.
- [25] C.T. Chien, S.S. Li, W.J. Lai, Y.C. Yeh, H.A. Chen, I.S. Chen, L.C. Chen, K.H. Chen, T. Nemoto, S. Isoda, M. Chen, T. Fujita, G. Eda, H. Yamaguchi, M. Chhowalla, C.W. Chen, Tunable photoluminescence from graphene oxide, *Angew Chem Int Ed Engl* 51(27) (2012) 6662-6.

- [26] J. Qian, D. Wang, F.H. Cai, W. Xi, L. Peng, Z.F. Zhu, H. He, M.L. Hu, S. He, Observation of multiphoton-induced fluorescence from graphene oxide nanoparticles and applications in in vivo functional bioimaging, *Angew Chem Int Ed Engl* 51(42) (2012) 10570-5.
- [27] J.L. Li, H.C. Bao, X.L. Hou, L. Sun, X.G. Wang, M. Gu, Graphene oxide nanoparticles as a nonbleaching optical probe for two-photon luminescence imaging and cell therapy, *Angew Chem Int Ed Engl* 51(8) (2012) 1830-4.
- [28] D.W. Jun Qian, Li Peng, Wang Xi, Fu-Hong Cai, Zhen-Feng Zhu, Hao He, Ming-Lie Hu, and Sailing He, Observation of Multiphoton-induced Fluorescence from Nano Graphene Oxide and Its Applications in In vitro and In vivo Bioimaging, (2012).
- [29] W. Denk, J.H. Strickler, W.W. Webb, Two-photon laser scanning fluorescence microscopy, *Science (New York, N.Y.)* 248(4951) (1990) 73-6.
- [30] J. Hong, J.Y. Han, H. Yoon, P. Joo, T. Lee, E. Seo, K. Char, B.S. Kim, Carbon-based layer-by-layer nanostructures: from films to hollow capsules, *Nanoscale* 3(11) (2011) 4515-31.
- [31] J. Hong, K. Char, B.-S. Kim, Hollow Capsules of Reduced Graphene Oxide Nanosheets Assembled on a Sacrificial Colloidal Particle, *The Journal of Physical Chemistry Letters* 1(24) (2010) 3442-3445.
- [32] L.L. del Mercato, F. Guerra, G. Lazzari, C. Nobile, C. Bucci, R. Rinaldi, Biocompatible multilayer capsules engineered with a graphene oxide derivative: synthesis, characterization and cellular uptake, *Nanoscale* 8(14) (2016) 7501-12.
- [33] H.R. Thomas, S.P. Day, W.E. Woodruff, C. Vallés, R.J. Young, I.A. Kinloch, G.W. Morley, J.V. Hanna, N.R. Wilson, J.P. Rourke, Deoxygenation of Graphene Oxide: Reduction or Cleaning?, *Chemistry of Materials* 25(18) (2013) 3580-3588.
- [34] D. Ma, L. Dong, M. Zhou, L. Zhu, The influence of oxidation debris containing in graphene oxide on the adsorption and electrochemical properties of 1,10-phenanthroline-5,6-dione, *Analyst* 141(9) (2016) 2761-6.
- [35] D.R. Dreyer, S. Park, C.W. Bielawski, R.S. Ruoff, The chemistry of graphene oxide, *Chem Soc Rev* 39(1) (2010) 228-40.
- [36] R. Vecchione, G. Iaccarino, P. Bianchini, R. Marotta, F. D'Autilia, V. Quagliariello, A. Diaspro, P.A. Netti, Ultrastable Liquid-Liquid Interface as Viable Route for Controlled Deposition of Biodegradable Polymer Nanocapsules, *Small (Weinheim an der Bergstrasse, Germany)* 12(22) (2016) 3005-13.

Chapter 5

Conclusions

In the recent years the huge wave of progress in science at the nanoscale has blossomed a new field of technologies applied to healthcare broadly named nanomedicine. In principle, the manipulation of materials at the nanometer level and the different properties that arise from there not only could overcome the limitations of the conventional therapeutic approaches but also revolutionize our idea of medicine. One of the main themes in nanomedicine is improving the efficacy of traditional therapeutic agents, especially in the treatment of cancer. To this purpose, the mainstream strategy is based on the design of delivery systems capable of positively affect the pharmacokinetic and biodistribution of drugs after their administration while reducing unpleasant side effects. In order to meet these fundamental requirements an ideal delivery system should first of all improve the solubility of the drugs where the most relevant therapeutics, especially anticancer agents, are highly hydrophobic molecules. At the same time it is crucial keeping the size of the delivery system small enough to minimize its clearance from the body and to exploit the ability of ≈ 100 nm particles to extravasate and enter the diseased tissue or the tumor. Even this relatively easy task is not obvious to carry out. In fact, delivery systems with a good compromise between dimensional features and a meaningful loading capacity have not been reported yet as a consolidated achievement by the literature. It is in this direction that the first efforts of this research work were devoted. Indeed, we developed a robust platform for the preparation of monodisperse oil-core nanocapsules capable of dissolving large amounts of hydrophobic drugs. Liquid

templates could virtually represent a viable way for the encapsulation of actives of importance for drug delivery. For this reason we strived to overcome some important issues in handling the high reactivity of these promising nanocapsular systems. In particular, an extremely versatile method for the electrostatic deposition of charged molecules at the interface of liquid nanocapsules has been developed. Starting from ultrastable secondary nanoemulsions, this technique allowed for the engineering of multifunctional polymeric nanocapsules made up of a number of diverse materials including: nature-derived polyelectrolytes, polysaccharides conjugated with peptides and graphene oxide nanosheets. We believe that the results reported in this work could actually contribute to boost the use of nanocapsules based on liquid templates as a useful tool for effective drug delivery.

As already mentioned, beyond the solubility issue there are other fundamental requirements to meet for improving the efficacy of conventional therapies. However, to date these higher purposes still remain challenging tasks. Too little is known to establish *a priori* if a strategy is better than another one. Ultimately, the processes underlying the interactions between the delivery system and the physiological environment are more sophisticated than what we can still predict. Hence, any study aimed at improving drug pharmacokinetics and minimizing its side effects is useful for the literature. In this work we tried to address these issues following two different approaches. In chapter 3 we presented a strategy to enhance the stability of nanocapsules and allow for a spatially controlled release mechanism. Basically, to reduce off-target toxicity and improve the performance of the drug it is crucial both preventing the systemic leakage of the drug and enabling the nanocapsules to release their payload only when they reach the target site could actually. The strategy we propose makes use of a single tool to address both the stability and the specific release issue. The central element is a Matrix Metalloproteases-2 responsive peptide that we embedded in our nanocapsules. Through a click chemistry

conjugation the peptide allowed to extend the nanocapsule stability in physiological media up to one month. Moreover, we tried to achieve a tumor selective release of the drug by a *stimuli*-responsive approach. Among the possible *stimuli* we chose the catalytic activity of these enzymes, which are typically overexpressed in tumor microenvironments. Preliminary results seem to encourage the use of a endogenous cues to trigger an on demand release. However, further biological studies are needed to validate the system.

A *stimuli*-responsive approach was also followed in the last part of this work where we presented an early study on the use of graphene oxide as a powerful tool for biomedical applications. The interest for this innovative material is rapidly increasing due to some intriguing properties including its intense optical adsorption in the near-infrared region of wavelengths. However, to date very little has been done for the integration of graphene oxide into nanosized drug delivery systems. In this context, we successfully coated oil-core nanocapsules with graphene oxide nanosheets and chitosan. The nanocapsules showed interesting optical properties including an intense near-infrared induced fluorescence which can be of real interest for biotechnology applications.

Moreover, we are currently exploring the potential of graphene oxide to transduce light into thermal energy to trigger the release of chemotherapeutic agents from the nanocapsules in a remote control fashion.

Taken altogether the results of this work of thesis encourage the use of oil-core nanocapsules as a viable tool for addressing the solubility issue of most therapeutics and implementing more sophisticated drug delivery systems of interest for nanomedicine.